Combination of the top-quark mass measurements from the Tevatron collider

T. Aaltonen,[12] V.M. Abazov,[48] B. Abbott,[112] B.S. Acharya,[31] M. Adams,[78] T. Adams,[74] G.D. Alexeev,[48] G. Alkhazov,[52] A. Alton[‡a],[96] B. Álvarez González[†z],[57] G. Alverson,[92] S. Amerio,[35] D. Amidei,[96] A. Anastassov[†x],[76] A. Annovi,[34] J. Antos,[53] G. Apollinari,[76] J.A. Appel,[76] T. Arisawa,[41] A. Artikov,[48] J. Asaadi,[119] W. Ashmanskas,[76] A. Askew,[74] S. Atkins,[89] B. Auerbach,[72] K. Augsten,[9] A. Aurisano,[119] C. Avila,[7] F. Azfar,[66] F. Badaud,[13] W. Badgett,[76] T. Bae,[43] L. Bagby,[76] B. Baldin,[76] D.V. Bandurin,[74] S. Banerjee,[31] A. Barbaro-Galtieri,[68] E. Barberis,[92] P. Baringer,[87] V.E. Barnes,[85] B.A. Barnett,[90] P. Barria[*d],[36] J.F. Bartlett,[76] P. Bartos,[53] U. Bassler,[18] M. Bauce[*b],[35] V. Bazterra,[78] A. Bean,[87] F. Bedeschi,[36] M. Begalli,[2] S. Behari,[90] L. Bellantoni,[76] G. Bellettini[*c],[36] J. Bellinger,[125] D. Benjamin,[109] A. Beretvas,[76] S.B. Beri,[29] G. Bernardi,[17] R. Bernhard,[22] I. Bertram,[61] M. Besançon,[18] R. Beuselinck,[63] P.C. Bhat,[76] S. Bhatia,[99] V. Bhatnagar,[29] A. Bhatti,[105] D. Bisello[*b],[35] I. Bizjak,[64] K.R. Bland,[122] G. Blazey,[79] S. Blessing,[74] K. Bloom,[100] B. Blumenfeld,[90] A. Bocci,[109] A. Bodek,[106] A. Boehnlein,[76] D. Boline,[107] E.E. Boos,[50] G. Borissov,[61] D. Bortoletto,[85] T. Bose,[91] J. Boudreau,[116] A. Boveia,[77] A. Brandt,[118] O. Brandt,[23] L. Brigliadori[*a],[33] R. Brock,[98] C. Bromberg,[98] A. Bross,[76] D. Brown,[17] J. Brown,[17] E. Brucken,[12] X.B. Bu,[76] J. Budagov,[48] H.S. Budd,[106] M. Buehler,[76] V. Buescher,[25] V. Bunichev,[50] S. Burdin[‡b],[61] K. Burkett,[76] G. Busetto[*b],[35] P. Bussey,[60] C.P. Buszello,[58] A. Buzatu,[4] A. Calamba,[115] C. Calancha,[56] E. Camacho-Pérez,[45] S. Camarda,[54] M. Campanelli,[64] M. Campbell,[96] F. Canelli,[77] B. Carls,[81] D. Carlsmith,[125] R. Carosi,[36] S. Carrillo[†m],[73] S. Carron,[76] B. Casal[†k],[57] M. Casarsa,[38] B.C.K. Casey,[76] H. Castilla-Valdez,[45] A. Castro[*a],[33] P. Catastini,[93] S. Caughron,[98] D. Cauz,[38] V. Cavaliere,[81] M. Cavalli-Sforza,[54] A. Cerri[†f],[68] L. Cerrito[†s],[64] S. Chakrabarti,[107] D. Chakraborty,[79] K.M. Chan,[84] A. Chandra,[121] E. Chapon,[18] G. Chen,[87] Y.C. Chen,[6] M. Chertok,[69] S. Chevalier-Théry,[18] G. Chiarelli,[36] G. Chlachidze,[76] F. Chlebana,[76] D.K. Cho,[117] K. Cho,[43] S.W. Cho,[44] S. Choi,[44] D. Chokheli,[48] B. Choudhary,[30] W.H. Chung,[125] Y.S. Chung,[106] S. Cihangir,[76] M.A. Ciocci[*d],[36] D. Claes,[100] A. Clark,[59] C. Clarke,[97] J. Clutter,[87] G. Compostella[*b],[35] M.E. Convery,[76] J. Conway,[69] M. Cooke,[76] W.E. Cooper,[76] M. Corbo,[76] M. Corcoran,[121] M. Cordelli,[34] F. Couderc,[18] M.-C. Cousinou,[15] C.A. Cox,[69] D.J. Cox,[69] F. Crescioli[*c],[36] A. Croc,[18] J. Cuevas[†z],[57] R. Culbertson,[76] D. Cutts,[117] D. Dagenhart,[76] A. Das,[67] N. d'Ascenzo[†w],[76] M. Datta,[76] G. Davies,[63] P. de Barbaro,[106] S.J. de Jong,[46, 47] E. De La Cruz-Burelo,[45] F. Déliot,[18] M. Dell'Orso[*c],[36] R. Demina,[106] L. Demortier,[105] M. Deninno,[33] D. Denisov,[76] S.P. Denisov,[51] M. d'Errico[*b],[35] S. Desai,[76] C. Deterre,[18] K. DeVaughan,[100] F. Devoto,[12] A. Di Canto[*c],[36] B. Di Ruzza,[76] H.T. Diehl,[76] M. Diesburg,[76] P.F. Ding,[65] J.R. Dittmann,[122] A. Dominguez,[100] S. Donati[*c],[36] P. Dong,[76] M. D'Onofrio,[62] M. Dorigo,[38] T. Dorigo,[35] A. Dubey,[30] L.V. Dudko,[50] D. Duggan,[101] A. Duperrin,[15] S. Dutt,[29] A. Dyshkant,[79] M. Eads,[100] K. Ebina,[41] D. Edmunds,[98] A. Elagin,[119] J. Ellison,[71] V.D. Elvira,[76] Y. Enari,[17] A. Eppig,[96] R. Erbacher,[69] S. Errede,[81] N. Ershaidat[†dd],[76] R. Eusebi,[119] H. Evans,[82] A. Evdokimov,[108] V.N. Evdokimov,[51] G. Facini,[92] S. Farrington,[66] M. Feindt,[24] L. Feng,[79] T. Ferbel,[106] J.P. Fernandez,[56] F. Fiedler,[25] R. Field,[73] F. Filthaut,[46, 47] W. Fisher,[98] H.E. Fisk,[76] G. Flanagan[†u],[76] R. Forrest,[69] M. Fortner,[79] H. Fox,[61] M.J. Frank,[122] M. Franklin,[93] J.C. Freeman,[76] S. Fuess,[76] Y. Funakoshi,[41] I. Furic,[73] M. Gallinaro,[105] J.E. Garcia,[59] A. Garcia-Bellido,[106] J.A. García-González,[45] G.A. García-Guerra[‡c],[45] A.F. Garfinkel,[85] P. Garosi[*d],[36] V. Gavrilov,[49] P. Gay,[13] W. Geng,[15, 98] D. Gerbaudo,[102] C.E. Gerber,[78] H. Gerberich,[81] E. Gerchtein,[76] Y. Gershtein,[101] S. Giagu,[37] V. Giakoumopoulou,[28] P. Giannetti,[36] K. Gibson,[116] C.M. Ginsburg,[76] G. Ginther,[76, 106] N. Giokaris,[28] P. Giromini,[34] G. Giurgiu,[90] V. Glagolev,[48] D. Glenzinski,[76] M. Gold,[103] D. Goldin,[119] N. Goldschmidt,[73] A. Golossanov,[76] G. Golovanov,[48] G. Gomez,[57] G. Gomez-Ceballos,[94] M. Goncharov,[94] O. González,[56] I. Gorelov,[103] A.T. Goshaw,[109] K. Goulianos,[105] A. Goussiou,[124] P.D. Grannis,[107] S. Greder,[19] H. Greenlee,[76] G. Grenier,[20] S. Grinstein,[54] Ph. Gris,[13] J.-F. Grivaz,[16] A. Grohsjean[‡d],[18] C. Grosso-Pilcher,[77] R.C. Group,[123, 76] S. Grünendahl,[76] M.W. Grünewald,[32] T. Guillemin,[16] J. Guimaraes da Costa,[93] G. Gutierrez,[76] P. Gutierrez,[112] S. Hagopian,[74] S.R. Hahn,[76] J. Haley,[92] E. Halkiadakis,[101] A. Hamaguchi,[40] J.Y. Han,[106] L. Han,[5] F. Happacher,[34] K. Hara,[42] K. Harder,[65] D. Hare,[101] M. Hare,[95] A. Harel,[106] R.F. Harr,[97] K. Hatakeyama,[122] J.M. Hauptman,[86] C. Hays,[66] J. Hays,[63] T. Head,[65] T. Hebbeker,[21] M. Heck,[24] D. Hedin,[79] H. Hegab,[113] J. Heinrich,[114] A.P. Heinson,[71] U. Heintz,[117] C. Hensel,[23] I. Heredia-De La Cruz,[45] M. Herndon,[125] K. Herner,[96] G. Hesketh[‡f],[65] S. Hewamanage,[122] M.D. Hildreth,[84] R. Hirosky,[123] T. Hoang,[74] J.D. Hobbs,[107] A. Hocker,[76] B. Hoeneisen,[11] J. Hogan,[121] M. Hohlfeld,[25] W. Hopkins[†g],[76] D. Horn,[24] S. Hou,[6] I. Howley,[118] Z. Hubacek,[9, 18] R.E. Hughes,[110]

arXiv:1207.1069v4 [hep-ex] 16 Nov 2012

M. Hurwitz,[77] U. Husemann,[72] N. Hussain,[4] M. Hussein,[98] J. Huston,[98] V. Hynek,[9] I. Iashvili,[104] Y. Ilchenko,[120] R. Illingworth,[76] G. Introzzi,[36] M. Iori[⋆f],[37] A.S. Ito,[76] A. Ivanov[†p],[69] S. Jabeen,[117] M. Jaffré,[16] E. James,[76] D. Jang,[115] A. Jayasinghe,[112] B. Jayatilaka,[109] E.J. Jeon,[43] M.S. Jeong,[44] R. Jesik,[63] S. Jindariani,[76] K. Johns,[67] E. Johnson,[98] M. Johnson,[76] A. Jonckheere,[76] M. Jones,[85] P. Jonsson,[63] K.K. Joo,[43] J. Joshi,[71] S.Y. Jun,[115] A.W. Jung,[76] T.R. Junk,[76] A. Juste,[55] K. Kaadze,[88] E. Kajfasz,[15] T. Kamon,[43, 119] P.E. Karchin,[97] D. Karmanov,[50] A. Kasmi,[122] P.A. Kasper,[76] Y. Kato[†o],[40] I. Katsanos,[100] R. Kehoe,[120] S. Kermiche,[15] W. Ketchum,[77] J. Keung,[114] N. Khalatyan,[76] A. Khanov,[113] A. Kharchilava,[104] Y.N. Kharzheev,[48] V. Khotilovich,[119] B. Kilminster,[76] D.H. Kim,[43] H.S. Kim,[43] J.E. Kim,[43] M.J. Kim,[34] S.B. Kim,[43] S.H. Kim,[42] Y.J. Kim,[43] Y.K. Kim,[77] N. Kimura,[41] M. Kirby,[76] I. Kiselevich,[49] S. Klimenko,[73] K. Knoepfel,[76] J.M. Kohli,[29] K. Kondo[⋆],[41] D.J. Kong,[43] J. Konigsberg,[73] A.V. Kotwal,[109] A.V. Kozelov,[51] J. Kraus,[99] M. Kreps,[24] J. Kroll,[114] D. Krop,[77] M. Kruse,[109] V. Krutelyov[†c],[119] T. Kuhr,[24] S. Kulikov,[51] A. Kumar,[104] A. Kupco,[10] M. Kurata,[42] T. Kurča,[20] V.A. Kuzmin,[50] S. Kwang,[77] A.T. Laasanen,[85] S. Lami,[36] S. Lammel,[76] S. Lammers,[82] M. Lancaster,[64] R.L. Lander,[69] G. Landsberg,[117] K. Lannon[†y],[110] A. Lath,[101] G. Latino[⋆d],[36] P. Lebrun,[20] T. LeCompte,[75] E. Lee,[119] H.S. Lee,[44] H.S. Lee[†q],[77] J.S. Lee,[43] S.W. Lee,[86] W.M. Lee,[76] S.W. Lee[†bb],[119] X. Lei,[67] J. Lellouch,[17] S. Leo[⋆c],[36] S. Leone,[36] J.D. Lewis,[76] H. Li,[14] L. Li,[71] Q.Z. Li,[76] J.K. Lim,[44] A. Limosani[†t],[109] C.-J. Lin,[68] D. Lincoln,[76] M. Lindgren,[76] J. Linnemann,[98] V.V. Lipaev,[51] E. Lipeles,[114] R. Lipton,[76] A. Lister,[59] D.O. Litvintsev,[76] C. Liu,[116] H. Liu,[120] H. Liu,[123] Q. Liu,[85] T. Liu,[76] Y. Liu,[5] A. Lobodenko,[52] S. Lockwitz,[72] A. Loginov,[72] M. Lokajicek,[10] R. Lopes de Sa,[107] H.J. Lubatti,[124] D. Lucchesi[⋆b],[35] J. Lueck,[24] P. Lujan,[68] P. Lukens,[76] R. Luna-Garcia[‡g],[45] G. Lungu,[105] A.L. Lyon,[76] J. Lys,[68] R. Lysak[†e],[53] A.K.A. Maciel,[1] R. Madar,[18] R. Madrak,[76] K. Maeshima,[76] P. Maestro[⋆d],[36] R. Magaña-Villalba,[45] S. Malik,[105] S. Malik,[100] V.L. Malyshev,[48] G. Manca[†a],[62] A. Manousakis-Katsikakis,[28] Y. Maravin,[88] F. Margaroli,[37] C. Marino,[24] M. Martínez,[54] J. Martínez-Ortega,[45] P. Mastrandrea,[37] K. Matera,[81] M.E. Mattson,[97] A. Mazzacane,[76] P. Mazzanti,[33] R. McCarthy,[107] K.S. McFarland,[106] C.L. McGivern,[65] P. McIntyre,[119] R. McNulty[†j],[62] A. Mehta,[62] P. Mehtala,[12] M.M. Meijer,[46, 47] A. Melnitchouk,[99] D. Menezes,[79] P.G. Mercadante,[3] M. Merkin,[50] C. Mesropian,[105] A. Meyer,[21] J. Meyer,[23] T. Miao,[76] F. Miconi,[19] D. Mietlicki,[96] A. Mitra,[6] H. Miyake,[42] S. Moed,[76] N. Moggi,[33] N.K. Mondal,[31] M.N. Mondragon[†m],[76] C.S. Moon,[43] R. Moore,[76] M.J. Morello[⋆e],[36] J. Morlock,[24] P. Movilla Fernandez,[76] A. Mukherjee,[76] M. Mulhearn,[123] Th. Muller,[24] P. Murat,[76] M. Mussini[⋆a],[33] J. Nachtman[†n],[76] Y. Nagai,[42] J. Naganoma,[41] E. Nagy,[15] M. Naimuddin,[30] I. Nakano,[39] A. Napier,[95] M. Narain,[117] R. Nayyar,[67] H.A. Neal,[96] J.P. Negret,[7] J. Nett,[119] C. Neu,[123] M.S. Neubauer,[81] P. Neustroev,[52] J. Nielsen[†d],[68] L. Nodulman,[75] S.Y. Noh,[43] O. Norniella,[81] T. Nunnemann,[26] L. Oakes,[66] S.H. Oh,[109] Y.D. Oh,[43] I. Oksuzian,[123] T. Okusawa,[40] R. Orava,[12] J. Orduna,[121] L. Ortolan,[54] N. Osman,[15] J. Osta,[84] M. Padilla,[71] S. Pagan Griso[⋆b],[35] C. Pagliarone,[38] A. Pal,[118] E. Palencia[†f],[57] V. Papadimitriou,[76] A.A. Paramonov,[75] N. Parashar,[83] V. Parihar,[117] S.K. Park,[44] R. Partridge[‡e],[117] N. Parua,[82] J. Patrick,[76] A. Patwa,[108] G. Pauletta[⋆g],[38] M. Paulini,[115] C. Paus,[94] D.E. Pellett,[69] B. Penning,[76] A. Penzo,[38] M. Perfilov,[50] Y. Peters,[65] K. Petridis,[65] G. Petrillo,[106] P. Pétroff,[16] T.J. Phillips,[109] G. Piacentino,[36] E. Pianori,[114] J. Pilot,[110] K. Pitts,[81] C. Plager,[70] M.-A. Pleier,[108] P.L.M. Podesta-Lerma[‡h],[45] V.M. Podstavkov,[76] L. Pondrom,[125] A.V. Popov,[51] S. Poprocki[†g],[76] K. Potamianos,[85] A. Pranko,[68] M. Prewitt,[121] D. Price,[82] N. Prokopenko,[51] F. Prokoshin[†cc],[48] F. Ptohos[†h],[34] G. Punzi[⋆c],[36] J. Qian,[96] A. Quadt,[23] B. Quinn,[99] A. Rahaman,[116] V. Ramakrishnan,[125] M.S. Rangel,[1] K. Ranjan,[30] N. Ranjan,[85] P.N. Ratoff,[61] I. Razumov,[51] I. Redondo,[56] P. Renkel,[120] P. Renton,[66] M. Rescigno,[37] T. Riddick,[64] F. Rimondi[⋆a],[33] I. Ripp-Baudot,[19] L. Ristori,[36, 76] F. Rizatdinova,[113] A. Robson,[60] T. Rodrigo,[57] T. Rodriguez,[114] E. Rogers,[81] S. Rolli[†i],[95] M. Rominsky,[76] R. Roser,[76] A. Ross,[61] C. Royon,[18] P. Rubinov,[76] R. Ruchti,[84] F. Ruffini[⋆d],[36] A. Ruiz,[57] J. Russ,[115] V. Rusu,[76] A. Safonov,[119] G. Sajot,[14] W.K. Sakumoto,[106] Y. Sakurai,[41] P. Salcido,[79] A. Sánchez-Hernández,[45] M.P. Sanders,[26] L. Santi[⋆g],[38] A.S. Santos[‡i],[1] K. Sato,[42] G. Savage,[76] V. Saveliev[†w],[76] A. Savoy-Navarro[†aa],[76] L. Sawyer,[89] T. Scanlon,[63] R.D. Schamberger,[107] Y. Scheglov,[52] H. Schellman,[80] P. Schlabach,[76] S. Schlobohm,[124] A. Schmidt,[24] E.E. Schmidt,[76] C. Schwanenberger,[65] T. Schwarz,[76] R. Schwienhorst,[98] L. Scodellaro,[57] A. Scribano[⋆d],[36] F. Scuri,[36] S. Seidel,[103] Y. Seiya,[40] J. Sekaric,[87] A. Semenov,[48] H. Severini,[112] F. Sforza[⋆d],[36] E. Shabalina,[23] S.Z. Shalhout,[69] V. Shary,[18] S. Shaw,[98] A.A. Shchukin,[51] T. Shears,[62] P.F. Shepard,[116] M. Shimojima[†v],[42] R.K. Shivpuri,[30] M. Shochet,[77] I. Shreyber-Tecker,[49] V. Simak,[9] A. Simonenko,[48] P. Sinervo,[4] P. Skubic,[112] P. Slattery,[106] K. Sliwa,[95] D. Smirnov,[84] J.R. Smith,[69] K.J. Smith,[104] F.D. Snider,[76] G.R. Snow,[100] J. Snow,[111] S. Snyder,[108] A. Soha,[76] S. Söldner-Rembold,[65] H. Song,[116] L. Sonnenschein,[21] V. Sorin,[54] K. Soustruznik,[8] P. Squillacioti[⋆d],[36] R. St. Denis,[60] M. Stancari,[76] J. Stark,[14] B. Stelzer,[4] O. Stelzer-Chilton,[4] D. Stentz[†x],[76] D.A. Stoyanova,[51] M. Strauss,[112] J. Strologas,[103] G.L. Strycker,[96] Y. Sudo,[42] A. Sukhanov,[76] I. Suslov,[48] L. Suter,[65] P. Svoisky,[112] M. Takahashi,[65] K. Takemasa,[42] Y. Takeuchi,[42] J. Tang,[77] M. Tecchio,[96] P.K. Teng,[6] J. Thom[†g],[76]

J. Thome,[115] G.A. Thompson,[81] E. Thomson,[114] M. Titov,[18] D. Toback,[119] S. Tokar,[53] V.V. Tokmenin,[48]
K. Tollefson,[98] T. Tomura,[42] D. Tonelli,[76] S. Torre,[34] D. Torretta,[76] P. Totaro,[35] M. Trovato[⋆e],[36] Y.-T. Tsai,[106]
K. Tschann-Grimm,[107] D. Tsybychev,[107] B. Tuchming,[18] C. Tully,[102] F. Ukegawa,[42] S. Uozumi,[43] L. Uvarov,[52]
S. Uvarov,[52] S. Uzunyan,[79] R. Van Kooten,[82] W.M. van Leeuwen,[46] N. Varelas,[78] A. Varganov,[96] E.W. Varnes,[67]
I.A. Vasilyev,[51] F. Vázquez[†m],[73] G. Velev,[76] C. Vellidis,[76] P. Verdier,[20] A.Y. Verkheev,[48] L.S. Vertogradov,[48]
M. Verzocchi,[76] M. Vesterinen,[65] M. Vidal,[85] I. Vila,[57] D. Vilanova,[18] R. Vilar,[57] J. Vizán,[57] M. Vogel,[103]
P. Vokac,[9] G. Volpi,[34] P. Wagner,[114] R.L. Wagner,[76] H.D. Wahl,[74] T. Wakisaka,[40] R. Wallny,[70] M.H.L.S. Wang,[76]
S.M. Wang,[6] A. Warburton,[4] J. Warchol,[84] D. Waters,[64] G. Watts,[124] M. Wayne,[84] J. Weichert,[25]
L. Welty-Rieger,[80] W.C. Wester III,[76] A. White,[118] D. Whiteson[†b],[114] F. Wick,[24] D. Wicke,[27] A.B. Wicklund,[75]
E. Wicklund,[76] S. Wilbur,[77] H.H. Williams,[114] M.R.J. Williams,[61] G.W. Wilson,[87] J.S. Wilson,[110] P. Wilson,[76]
B.L. Winer,[110] P. Wittich[†g],[76] M. Wobisch,[89] S. Wolbers,[76] H. Wolfe,[110] D.R. Wood,[92] T. Wright,[96] X. Wu,[59]
Z. Wu,[122] T.R. Wyatt,[65] Y. Xie,[76] R. Yamada,[76] K. Yamamoto,[40] D. Yamato,[40] S. Yang,[5] T. Yang,[76]
U.K. Yang[†r],[77] W.-C. Yang,[65] Y.C. Yang,[43] W.-M. Yao,[68] T. Yasuda,[76] Y.A. Yatsunenko,[48] W. Ye,[107] Z. Ye,[76]
G.P. Yeh,[76] H. Yin,[76] K. Yi[†n],[76] K. Yip,[108] J. Yoh,[76] K. Yorita,[41] T. Yoshida[†l],[40] S.W. Youn,[76] G.B. Yu,[109]
I. Yu,[43] J.M. Yu,[96] S.S. Yu,[76] J.C. Yun,[76] A. Zanetti,[38] Y. Zeng,[109] J. Zennamo,[104] T. Zhao,[124] T.G. Zhao,[65]
B. Zhou,[96] C. Zhou,[109] J. Zhu,[96] M. Zielinski,[106] D. Zieminska,[82] L. Zivkovic,[117] and S. Zucchelli[⋆a33]
(CDF and D0 Collaborations [†] [‡])

[1]LAFEX, Centro Brasileiro de Pesquisas Físicas, Rio de Janeiro, Brazil
[2]Universidade do Estado do Rio de Janeiro, Rio de Janeiro, Brazil
[3]Universidade Federal do ABC, Santo André, Brazil
[4]Institute of Particle Physics: McGill University, Montréal, Québec,
Canada H3A 2T8; Simon Fraser University, Burnaby, British Columbia,
Canada V5A 1S6; University of Toronto, Toronto, Ontario,
Canada M5S 1A7; and TRIUMF, Vancouver, British Columbia, Canada V6T 2A3
[5]University of Science and Technology of China, Hefei, People's Republic of China
[6]Institute of Physics, Academia Sinica, Taipei, Taiwan 11529, Republic of China
[7]Universidad de los Andes, Bogotá, Colombia
[8]Charles University, Faculty of Mathematics and Physics,
Center for Particle Physics, Prague, Czech Republic
[9]Czech Technical University in Prague, Prague, Czech Republic
[10]Center for Particle Physics, Institute of Physics,
Academy of Sciences of the Czech Republic, Prague, Czech Republic
[11]Universidad San Francisco de Quito, Quito, Ecuador
[12]Division of High Energy Physics, Department of Physics,
University of Helsinki and Helsinki Institute of Physics, FIN-00014, Helsinki, Finland
[13]LPC, Université Blaise Pascal, CNRS/IN2P3, Clermont, France
[14]LPSC, Université Joseph Fourier Grenoble 1, CNRS/IN2P3,
Institut National Polytechnique de Grenoble, Grenoble, France
[15]CPPM, Aix-Marseille Université, CNRS/IN2P3, Marseille, France
[16]LAL, Université Paris-Sud, CNRS/IN2P3, Orsay, France
[17]LPNHE, Universités Paris VI and VII, CNRS/IN2P3, Paris, France
[18]CEA, Irfu, SPP, Saclay, France
[19]IPHC, Université de Strasbourg, CNRS/IN2P3, Strasbourg, France
[20]IPNL, Université Lyon 1, CNRS/IN2P3, Villeurbanne, France and Université de Lyon, Lyon, France
[21]III. Physikalisches Institut A, RWTH Aachen University, Aachen, Germany
[22]Physikalisches Institut, Universität Freiburg, Freiburg, Germany
[23]II. Physikalisches Institut, Georg-August-Universität Göttingen, Göttingen, Germany
[24]Institut für Experimentelle Kernphysik, Karlsruhe Institute of Technology, D-76131 Karlsruhe, Germany
[25]Institut für Physik, Universität Mainz, Mainz, Germany
[26]Ludwig-Maximilians-Universität München, München, Germany
[27]Fachbereich Physik, Bergische Universität Wuppertal, Wuppertal, Germany
[28]University of Athens, 157 71 Athens, Greece
[29]Panjab University, Chandigarh, India
[30]Delhi University, Delhi, India
[31]Tata Institute of Fundamental Research, Mumbai, India
[32]University College Dublin, Dublin, Ireland
[33]Istituto Nazionale di Fisica Nucleare Bologna, [⋆a]University of Bologna, I-40127 Bologna, Italy
[34]Laboratori Nazionali di Frascati, Istituto Nazionale di Fisica Nucleare, I-00044 Frascati, Italy
[35]Istituto Nazionale di Fisica Nucleare, Sezione di Padova-Trento, [⋆b]University of Padova, I-35131 Padova, Italy

[36]Istituto Nazionale di Fisica Nucleare Pisa, [c]University of Pisa,
[d]University of Siena and [e]Scuola Normale Superiore, I-56127 Pisa, Italy
[37]Istituto Nazionale di Fisica Nucleare, Sezione di Roma 1,
[f]Sapienza Università di Roma, I-00185 Roma, Italy
[38]Istituto Nazionale di Fisica Nucleare Trieste/Udine,
I-34100 Trieste, [g]University of Udine, I-33100 Udine, Italy
[39]Okayama University, Okayama 700-8530, Japan
[40]Osaka City University, Osaka 588, Japan
[41]Waseda University, Tokyo 169, Japan
[42]University of Tsukuba, Tsukuba, Ibaraki 305, Japan
[43]Center for High Energy Physics: Kyungpook National University,
Daegu 702-701, Korea; Seoul National University, Seoul 151-742,
Korea; Sungkyunkwan University, Suwon 440-746,
Korea; Korea Institute of Science and Technology Information,
Daejeon 305-806, Korea; Chonnam National University, Gwangju 500-757,
Korea; Chonbuk National University, Jeonju 561-756, Korea
[44]Korea Detector Laboratory, Korea University, Seoul, Korea
[45]CINVESTAV, Mexico City, Mexico
[46]Nikhef, Science Park, Amsterdam, the Netherlands
[47]Radboud University Nijmegen, Nijmegen, the Netherlands
[48]Joint Institute for Nuclear Research, Dubna, Russia
[49]Institute for Theoretical and Experimental Physics, Moscow, Russia
[50]Moscow State University, Moscow, Russia
[51]Institute for High Energy Physics, Protvino, Russia
[52]Petersburg Nuclear Physics Institute, St. Petersburg, Russia
[53]Comenius University, 842 48 Bratislava, Slovakia; Institute of Experimental Physics, 040 01 Kosice, Slovakia
[54]Institut de Fisica d'Altes Energies, ICREA, Universitat Autonoma de Barcelona, E-08193, Bellaterra (Barcelona), Spain
[55]Institució Catalana de Recerca i Estudis Avançats (ICREA) and Institut de Física d'Altes Energies (IFAE), Barcelona, Spain
[56]Centro de Investigaciones Energeticas Medioambientales y Tecnologicas, E-28040 Madrid, Spain
[57]Instituto de Fisica de Cantabria, CSIC-University of Cantabria, 39005 Santander, Spain
[58]Uppsala University, Uppsala, Sweden
[59]University of Geneva, CH-1211 Geneva 4, Switzerland
[60]Glasgow University, Glasgow G12 8QQ, United Kingdom
[61]Lancaster University, Lancaster LA1 4YB, United Kingdom
[62]University of Liverpool, Liverpool L69 7ZE, United Kingdom
[63]Imperial College London, London SW7 2AZ, United Kingdom
[64]University College London, London WC1E 6BT, United Kingdom
[65]The University of Manchester, Manchester M13 9PL, United Kingdom
[66]University of Oxford, Oxford OX1 3RH, United Kingdom
[67]University of Arizona, Tucson, Arizona 85721, USA
[68]Ernest Orlando Lawrence Berkeley National Laboratory, Berkeley, California 94720, USA
[69]University of California, Davis, Davis, California 95616, USA
[70]University of California, Los Angeles, Los Angeles, California 90024, USA
[71]University of California Riverside, Riverside, California 92521, USA
[72]Yale University, New Haven, Connecticut 06520, USA
[73]University of Florida, Gainesville, Florida 32611, USA
[74]Florida State University, Tallahassee, Florida 32306, USA
[75]Argonne National Laboratory, Argonne, Illinois 60439, USA
[76]Fermi National Accelerator Laboratory, Batavia, Illinois 60510, USA
[77]Enrico Fermi Institute, University of Chicago, Chicago, Illinois 60637, USA
[78]University of Illinois at Chicago, Chicago, Illinois 60607, USA
[79]Northern Illinois University, DeKalb, Illinois 60115, USA
[80]Northwestern University, Evanston, Illinois 60208, USA
[81]University of Illinois, Urbana, Illinois 61801, USA
[82]Indiana University, Bloomington, Indiana 47405, USA
[83]Purdue University Calumet, Hammond, Indiana 46323, USA
[84]University of Notre Dame, Notre Dame, Indiana 46556, USA
[85]Purdue University, West Lafayette, Indiana 47907, USA
[86]Iowa State University, Ames, Iowa 50011, USA
[87]University of Kansas, Lawrence, Kansas 66045, USA
[88]Kansas State University, Manhattan, Kansas 66506, USA
[89]Louisiana Tech University, Ruston, Louisiana 71272, USA
[90]The Johns Hopkins University, Baltimore, Maryland 21218, USA
[91]Boston University, Boston, Massachusetts 02215, USA

[92] Northeastern University, Boston, Massachusetts 02115, USA
[93] Harvard University, Cambridge, Massachusetts 02138, USA
[94] Massachusetts Institute of Technology, Cambridge, Massachusetts 02139, USA
[95] Tufts University, Medford, Massachusetts 02155, USA
[96] University of Michigan, Ann Arbor, Michigan 48109, USA
[97] Wayne State University, Detroit, Michigan 48201, USA
[98] Michigan State University, East Lansing, Michigan 48824, USA
[99] University of Mississippi, University, Mississippi 38677, USA
[100] University of Nebraska, Lincoln, Nebraska 68588, USA
[101] Rutgers University, Piscataway, New Jersey 08855, USA
[102] Princeton University, Princeton, New Jersey 08544, USA
[103] University of New Mexico, Albuquerque, New Mexico 87131, USA
[104] State University of New York, Buffalo, New York 14260, USA
[105] The Rockefeller University, New York, New York 10065, USA
[106] University of Rochester, Rochester, New York 14627, USA
[107] State University of New York, Stony Brook, New York 11794, USA
[108] Brookhaven National Laboratory, Upton, New York 11973, USA
[109] Duke University, Durham, North Carolina 27708, USA
[110] The Ohio State University, Columbus, Ohio 43210, USA
[111] Langston University, Langston, Oklahoma 73050, USA
[112] University of Oklahoma, Norman, Oklahoma 73019, USA
[113] Oklahoma State University, Stillwater, Oklahoma 74078, USA
[114] University of Pennsylvania, Philadelphia, Pennsylvania 19104, USA
[115] Carnegie Mellon University, Pittsburgh, Pennsylvania 15213, USA
[116] University of Pittsburgh, Pittsburgh, Pennsylvania 15260, USA
[117] Brown University, Providence, Rhode Island 02912, USA
[118] University of Texas, Arlington, Texas 76019, USA
[119] Texas A&M University, College Station, Texas 77843, USA
[120] Southern Methodist University, Dallas, Texas 75275, USA
[121] Rice University, Houston, Texas 77005, USA
[122] Baylor University, Waco, Texas 76798, USA
[123] University of Virginia, Charlottesville, Virginia 22904, USA
[124] University of Washington, Seattle, Washington 98195, USA
[125] University of Wisconsin, Madison, Wisconsin 53706, USA

The top quark is the heaviest known elementary particle, with a mass about 40 times larger than the mass of its isospin partner, the bottom quark. It decays almost 100% of the time to a W boson and a bottom quark. Using top-antitop pairs at the Tevatron proton-antiproton collider, the CDF and D0 Collaborations have measured the top quark's mass in different final states for integrated luminosities of up to 5.8 fb^{-1}. This paper reports on a combination of these measurements that results in a more precise value of the mass than any individual decay channel can provide. It describes the treatment of the systematic uncertainties and their correlations. The mass value determined is 173.18 ± 0.56 (stat) ± 0.75 (syst) GeV or 173.18 ± 0.94 GeV, which has a precision of $\pm 0.54\%$, making this the most precise determination of the top-quark mass.

[*] Deceased
[†] With CDF visitors from [†a] Istituto Nazionale di Fisica Nucleare, Sezione di Cagliari, 09042 Monserrato (Cagliari), Italy, [†b] University of California Irvine, Irvine, CA 92697, USA, [†c] University of California Santa Barbara, Santa Barbara, CA 93106, USA, [†d] University of California Santa Cruz, Santa Cruz, CA 95064, USA, [†e] Institute of Physics, Academy of Sciences of the Czech Republic, Czech Republic, [†f] CERN, CH-1211 Geneva, Switzerland, [†g] Cornell University, Ithaca, NY 14853, USA, [†h] University of Cyprus, Nicosia CY-1678, Cyprus, [†i] Office of Science, U.S. Department of Energy, Washington, DC 20585, USA, [†j] University College Dublin, Dublin 4, Ireland, [†k] ETH, 8092 Zurich, Switzerland, [†l] University of Fukui, Fukui City, Fukui Prefecture, Japan 910-0017, [†m] Universidad Iberoamericana, Mexico D.F., Mexico, [†n] University of Iowa, Iowa City, IA 52242, USA, [†o] Kinki University, Higashi-Osaka City, Japan 577-8502, [†p] Kansas State University, Manhattan, KS 66506, USA, [†q] Ewha Womans University, Seoul, 120-750, Korea, [†r] University of Manchester, Manchester M13 9PL, United Kingdom, [†s] Queen Mary, University of London, London, E1 4NS, United Kingdom, [†t] University of Melbourne, Victoria 3010, Australia, [†u] Muons, Inc., Batavia, IL 60510, USA, [†v] Nagasaki Institute of Applied Science, Nagasaki, Japan, [†w] National Research Nuclear University, Moscow, Russia, [†x] Northwestern University, Evanston, IL 60208, USA, [†y] University of Notre Dame, Notre Dame, IN 46556, USA, [†z] Universidad de Oviedo, E-33007 Oviedo, Spain, [†aa] CNRS-IN2P3, Paris, F-75205 France, [†bb] Texas Tech University, Lubbock, TX 79609, USA, [†cc] Universidad Tecnica Federico Santa Maria,

B. Top-quark mass origin and definitions

One of the fundamental properties of an elementary particle is its mass. In the SM, fermions acquire mass through interactions with the Higgs field [10]. Absolute values of these masses are not predicted by the SM. In theoretical calculations, a particle's mass can be defined in more than one way, and it depends on how higher-order terms in perturbative quantum chromodynamics (QCD) calculations are renormalized. In the modified minimal subtraction scheme ($\overline{\text{MS}}$), for example, the mass definition reflects short-distance effects, whereas in the pole-mass scheme the mass definition reflects long-distance effects [11]. The concept of the pole mass is not well defined since color confinement does not provide S-matrix poles at $m = m_t$ [12]. Direct mass measurements that are inputs to the combination described in this paper rely on Monte Carlo (MC) generators to extract m_t. Hence the measured mass corresponds in fact to the mass parameter in the MC. Work is proceeding to address the exact difference between the measured mass and the pole mass, as presented, for example, in Appendix C of Ref. [13]. One alternative way to address this problem is to extract m_t from a measurement of the $t\bar{t}$ cross section [14]. The D0 Collaboration has recently shown that the directly measured mass of the top quark is closer to the pole mass extracted from a measurement of the $t\bar{t}$ cross section than to an $\overline{\text{MS}}$ mass extracted in a similar way [14]. Hence, within the precision of theory and data, the directly measured m_t is best interpreted as the top-quark pole mass.

CPT invariance predicts that a particle and its antiparticle partner have the same mass. This has been checked for the top quark by the D0, CDF, and CMS Collaborations, and the masses are found to hold within the measurement uncertainties, with $\Delta m_t = m_t - m_{\bar{t}} = 0.84 \pm 1.87$ GeV [15], $\Delta m_t = -3.3 \pm 1.7$ GeV [16], and $\Delta m_t = -0.44 \pm 0.53$ GeV [17], respectively. Thus, the top-quark mass combination in this paper assumes $m_t = m_{\bar{t}}$.

C. Predictions based on the top-quark mass

The internal consistency of the SM can be tested by using different observables to predict the values of others and then to compare the expectations with their measured values. For example, the relation between the mass of the W boson (M_W) and $\sin^2\theta_W$ (the electroweak mixing angle) includes higher-order radiative corrections involving m_t, hence the smaller the uncertainty on the measured m_t; the stronger is the test of consistency.

Since 1997, the LEP Electroweak Working Group has used the observed top-quark and the W boson masses and other precision electroweak variables to extract constrains on the Higgs boson mass (M_H) in the SM [18]. This has been extended to the minimal supersymmetric standard model [19], and the GFITTER Collaboration has applied the technique to set limits on a wide variety

of theories beyond the SM [20]. Figure 3a shows the combined constraint attributable to M_W and m_t (as of March 2012) on the Higgs boson mass. Figure 3b shows the constraint from M_W and m_t separately (as of March 2012) on the Higgs boson mass, and a global constraint originating from all the other electroweak variables, showing the importance of the M_W and m_t variables to constrain the Higgs boson mass.
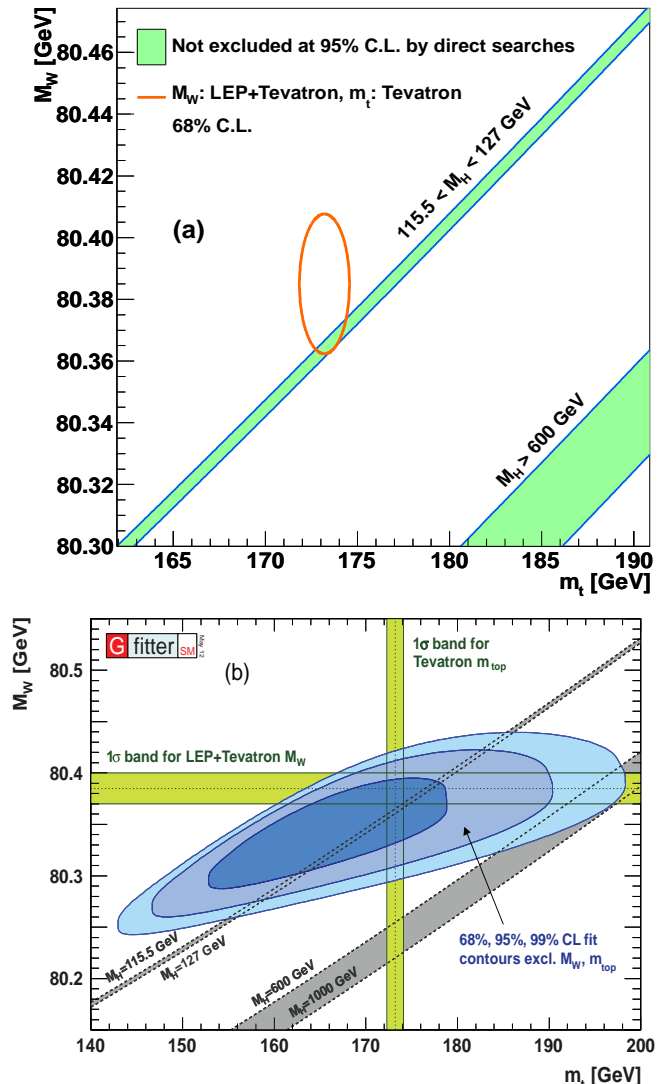
FIG. 3: Constraints from LEP and Tevatron measurements of M_W and m_t (Tevatron only) on M_H within the SM. The regions in the mass of the Higgs boson still allowed after the direct searches at LEP, Tevatron and LHC are also shown. From Ref. [20], the large countors (blue) indicate the constraints on the Higgs boson, from global fits to electroweak data without including the direct measurements of M_W and m_t from the Tevatron.

D. History of measurement of m_t

Before 1995, global fits to electroweak data from the CERN and SLAC e^+e^- colliders (LEP and SLC) and from other experiments produced estimates of m_t that

ranged from $\approx$ 90 GeV to $\approx$ 190 GeV [21]. At the time of the first observation of the top quark in 1995, the fits indicated a mass close to the current Tevatron value of m_t, but with an uncertainty of $\approx \pm 10\%$ and an assumption of 300 GeV mass of the Higgs boson [22]. CDF measured $m_t = 176 \pm 8(\text{stat}) \pm 10(\text{syst})$ GeV [4] (total uncertainty of 7%) and D0 measured $m_t = 199^{+19}_{-21}(\text{stat}) \pm 22(\text{syst})$ GeV [5] (total uncertainty of 15%).

Since then, the CDF and D0 Collaborations have developed many novel measurement techniques and published nearly 50 journal papers on their measurements of m_t. Recently, the CMS Collaboration at the Large Hadron Collider (LHC) published a measurement using 102 dilepton events [23] and finds $m_t = 175.5 \pm 4.6(\text{stat}) \pm 4.6(\text{syst})$ GeV (total uncertainty of 3.7%). The ATLAS Collaboration at the LHC has submitted a measurement of $m_t = 174.5 \pm 0.6 \pm 2.3$ GeV (total uncertainty of 1.4%) using nearly 12,000 lepton+jets events [24]. The most precise measurements from the Tevatron in a single decay channel use lepton+jets events, a matrix-element method as introduced in Ref. [25], and an *in situ* calibration of the jet energy scale. CDF's matrix-element measurement [26] uses 5.6 fb^{-1} of integrated luminosity to find $m_t = 173.00 \pm 0.65(\text{stat}) \pm 1.06(\text{syst})$ GeV (total uncertainty of 0.72%). D0's measurement [27] uses 3.6 fb^{-1} of integrated luminosity to obtain $m_t = 174.94 \pm 0.83(\text{stat}) \pm 1.24(\text{syst})$ GeV (total uncertainty of 0.85%). Figure 4 shows the publication history of the direct measurements of m_t at the Tevatron.

E. Overview of mass measurements

This paper reports on the combination of previously published measurements of m_t. Details of the analyses are therefore not repeated as this information is available in recent reviews [28], as well as in the publications of each of the results. We will, however, summarize the basic techniques used for the measurements.

The cross section for $t\bar{t}$ production in proton-antiproton ($p\bar{p}$) interactions at 1.96 TeV is $\approx$ 7.2 pb [29, 30]. The mean transverse momentum (p_T) of the $t\bar{t}$ system at parton level is $\approx$ 20 GeV, which is attributed to initial-state radiation (i.e., gluon emission). The mean transverse momentum of the top quarks at parton level is $\approx$ 95 GeV [31]. Top quarks have a lifetime of $\approx 0.3 \times 10^{-24}$ s [32, 33], which is an order of magnitude smaller than the time scale for parton evolution and hadronization. Hence, when top quarks decay, they transfer their kinematic characteristics to the W boson and b quark, and the measured energy-momentum four-vectors of the final-state particles can be used to reconstruct the mass of the top quark, except for the presence of initial or final-state radiation.

In alljets events, the four-vector of every jet emerging from quarks can be reconstructed, but neutrinos emitted in semileptonic decays of b quarks and jet energy resolution effects will lead to lost energy. In lepton+jets events, the momentum of the neutrino from the $W \to \ell\nu_\ell$ decay is not detected. The transverse component can be inferred from the negative of the vector sum of all transverse momenta of particles detected in the calorimeter and muon detectors. We estimate the longitudinal momentum of ν_ℓ by constraining the mass of the charged lepton and neutrino system to the world average value of M_W [7]. We also use M_W to choose the two light jets from $W \to q\bar{q}'$ decay, and we use that information for an *in situ* calibration of jet energies. In dilepton events, the analysis is more complicated because there are two final-state neutrinos from the leptonic decays of both W bosons. Therefore, the longitudinal and transverse-momentum components of the neutrinos cannot be determined without the application of more sophisticated tools. These involve assuming a value for m_t to solve the event kinematics and assigning a weight to each m_t hypothesis to determine the most likely value of m_t consistent with the hypothesis that the event is a $t\bar{t}$ event.

A major issue in $t\bar{t}$ final-state reconstruction is the correct mapping of the reconstructed objects to the partons from the decays of the top quark and W boson. The problem arises because often the jet charge and flavor cannot be uniquely determined. This creates combinatorial ambiguities in the $t\bar{t}$ event reconstruction that vary from 90 possible jet-to-parton assignments for the alljets final state to 2 in the dilepton channel. In the lepton+jets and dilepton final states, additional ambiguities may arise from multiple kinematical solutions for the longitudinal component of the neutrino momentum.

Two methods are used to measure the value of m_t. In the first method, the reconstructed mass distribution in data, or a variable correlated with m_t, such as the decay length of the B hadron or the transverse momentum of a lepton, is compared to template distributions composed of contributions from background and simulation of $t\bar{t}$ events. One template is used to represent background and another for each putative value of m_t. The second method uses event probabilities based on the LO matrix element for the production of $t\bar{t}$. For each event, a probability is calculated as a function of m_t that this event is from $t\bar{t}$ production, as based on the corresponding production and decay matrix element. Detector resolution is taken into account in the calculation of these probabilities through transfer functions that correlate parton-level energies and their measured values. The value of m_t is then extracted from the joint probability calculated for all selected events, based on the probability for signal and background (also defined through its matrix element). This method produces the most accurate results, but the computations are time-consuming.

F. Combination overview

This paper describes the combination of statistically independent top-quark mass measurements from
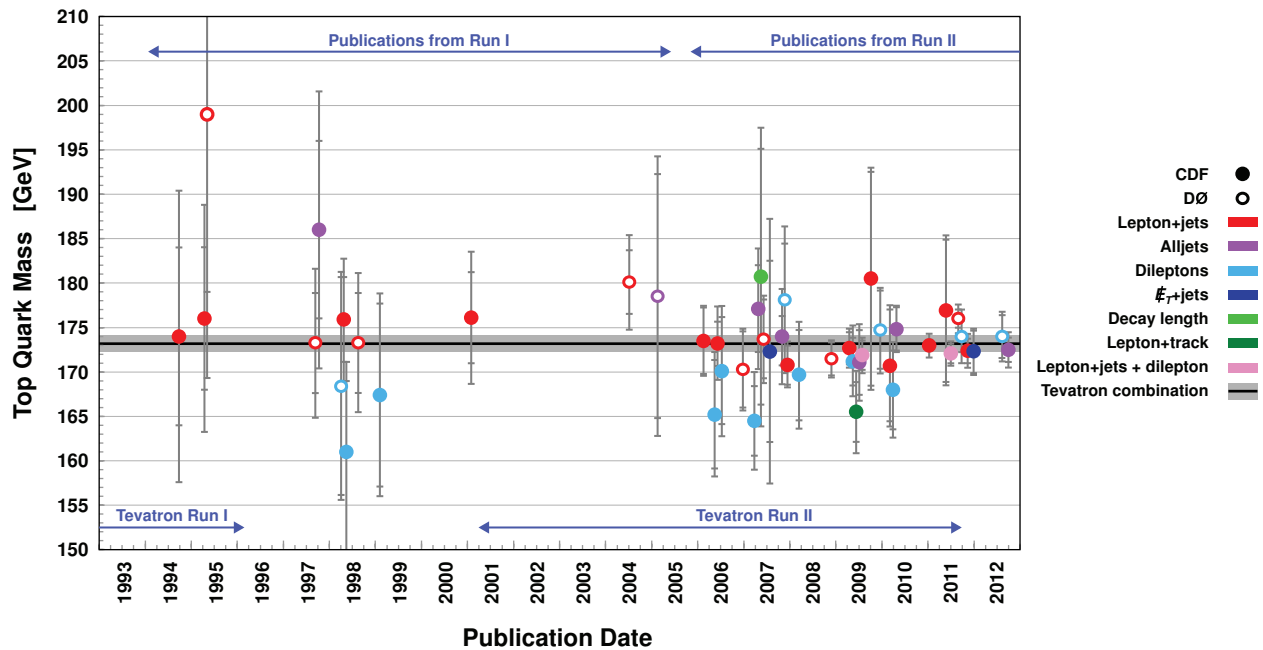
FIG. 4: The CDF and D0 published direct measurements of the top-quark mass as a function of time.

the Fermilab Tevatron Collider. Measurements are independent if they are based on different data sets, e.g., from CDF and from D0, or from Tevatron Run I (1992–1996) and Run II (2001–2011). They are also independent within one data set if the event selections are designed to be exclusive; i.e., no event can pass more than one category of selections. At times, more than one measurement is published using the same data and decay channel. In this situation, the result with smallest overall uncertainty is chosen for the combination. Twelve measurements are used in the combination described here, eight from the CDF collaboration and four from D0. These comprise five lepton+jets measurements (CDF and D0, Run II and Run I, and a CDF Run II result based on the decay length of B hadrons); two alljets measurements (CDF Run II and Run I); four dilepton measurements (CDF and D0, Run II and Run I); and a $\not{E}_T$+jets measurement (CDF Run II). We combine these measurements using an analytic method called the best linear unbiased estimator (BLUE) [34–36]. This technique forms a linear combination of the separate unbiased mass measurements to produce the best estimate of m_t with the smallest uncertainty. This procedure follows a series of 11 such mass combinations presented in [37–47], updated each year since 2004 as new measurements of m_t became available. The combination presented here is the first to be published in a peer-reviewed journal.

II. INPUTS TO THE COMBINATION

A. The independent mass measurements

The mass measurements included in the combination are shown in Table I [26, 27, 48–57]. These 12 channels are chosen because they are statistically independent, which maximizes the improvement in the combination, and because enough information is available to separate the components of systematic uncertainty for proper treatment in the combination.

The D0 measurement from 2005 in the alljets channel (Run I) [58] of $m_t = 178.5 \pm 13.7(\text{stat}) \pm 7.7(\text{syst})$ GeV (total uncertainty of 8.8%) is not included in the combination because some subcomponents of the systematic uncertainty are not available.

The CDF measurement from Run II based on decay-length analysis [57] differs from the others in that it uses the mean decay length of B hadrons in b-tagged lepton+jets events as the m_t-sensitive variable. It is independent of energy information in the calorimeter, and its main source of systematic uncertainty is uncorrelated with the dominant ones from the jet energy scale calibration in other measurements. This measurement of m_t is essentially uncorrelated with the higher precision CDF result from the lepton+jets channel. The overlap between the data samples used for the decay-length method and the lepton+jets sample has therefore no effect.

B. Data

The data were collected with the CDF [59] and D0 [60, 61] detectors at the Tevatron $p\bar{p}$ collider at Fermilab between 1992 and 2009. The Tevatron "center-

TABLE I: Top-quark mass measurements used as input to determine the combined value of m_t from the Tevatron and the combined result.

Decay channel or method	Tevatron period	Experiment	Integrated luminosity [fb^{-1}]	Number of events	Background [%]	m_t [GeV]	Uncertainty on m_t [%]	Reference
Lepton+jets	Run II	CDF	5.6	1087	17	$173.00 \pm 0.65 \pm 1.06$	0.72	[26]
Lepton+jets	Run II	D0	3.6	615	27	$174.94 \pm 0.83 \pm 1.24$	0.85	[27]
Lepton+jets	Run I	CDF	0.1	76	54	$176.1 \pm 5.1 \pm 5.3$	4.2	[48]
Lepton+jets	Run I	D0	0.1	22	22	$180.1 \pm 3.6 \pm 3.9$	2.9	[49]
Alljets	Run II	CDF	5.8	2856	71	$172.47 \pm 1.43 \pm 1.40$	1.2	[50]
Alljets	Run I	CDF	0.1	136	79	$186.0 \pm 10.0 \pm 5.7$	6.2	[51]
Dileptons	Run II	CDF	5.6	392	23	$170.28 \pm 1.95 \pm 3.13$	2.2	[52]
Dileptons	Run II	D0	5.3	415	21	$174.00 \pm 2.36 \pm 1.44$	1.6	[53]
Dileptons	Run I	CDF	0.1	8	16	$167.4 \pm 10.3 \pm 4.9$	6.8	[54]
Dileptons	Run I	D0	0.1	6	25	$168.4 \pm 12.3 \pm 3.6$	7.6	[55]
$\not{E}_T$+jets	Run II	CDF	5.7	1432	32	$172.32 \pm 1.80 \pm 1.82$	1.5	[56]
Decay length	Run II	CDF	1.9	375	30	$166.90 \pm 9.00 \pm 2.82$	5.7	[57]
Combination			≤ 5.8	7420	44	$173.18 \pm 0.56 \pm 0.75$	0.54	

of-mass" energy was 1.8 TeV in Run I from 1992 to 1996 and 1.96 TeV in Run II from 2001. A silicon microstrip tracker around the beam pipe at the center of each detector was used to reconstruct charged-particle tracks (only in Run II at D0). Tracks spatially matched to calorimeter jets are checked for originating from a secondary vertex, or for evidence that they originate from decays of long-lived heavy-flavor hadrons containing b quarks from the decay of top quarks [59, 62]. Electrons and jets produce particle showers in the calorimeters, and the collected information is used to measure their energies. Muons traverse the calorimeters and outer muon detectors that are used to measure their tracks. Both CDF and D0 have central axial magnetic fields in the tracking region (D0 only in Run II), in which the momenta of charged particles are determined from the curvature of their tracks. The CDF magnet has a diameter of 3 m and extends 4.8 m along the beam line, with a field strength of 1.4 T, and the D0 magnet has a diameter of 1.0 m and length of 2.7 m to fit inside the Run I calorimeter with a field strength of 2.0 T. The CDF detector's larger tracking volume with a higher density of measurements gives better transverse-momentum resolution for charged-particle tracks. The transverse-momentum resolution is $\approx 3.5\%$ at CDF and $\approx 10\%$ at D0 for a muon with $p_T = 50$ GeV. The trigger and event-selection criteria depend on the $t\bar{t}$ final states, details of which appear in the publications listed in Table I. The experiments collected $\mathcal{O}(10^{14})$ hard collisions, from which 7420 events are selected because they have the characteristics expected for $t\bar{t}$ pairs, of which $\approx 56\%$ are expected to be true $t\bar{t}$ events.

C. Models for $t\bar{t}$ signal

The $t\bar{t}$ signal in Run I was simulated using the LO generator HERWIG [64] with the MRSD$'_0$ [65] and CTEQ4M [66] parton distribution functions (PDF) used by CDF and D0, respectively. The HERWIG generator implements the hard-scattering processes $q\bar{q}{\rightarrow}t\bar{t}$ and

$gg{\rightarrow}t\bar{t}$, adding initial-state and final-state radiation through leading-log QCD evolution [67]. The top quark and W boson in HERWIG decay according to the branching fractions listed by the Particle Data Group [7], and the final-state partons are subsequently fragmented into jets. The MC events are then processed through a fast simulation or a GEANT model [68] of the detectors and then through event reconstruction programs.

For the $t\bar{t}$ signal in Run II, CDF uses PYTHIA [69] with the CTEQ5L [70] PDF, and D0 uses the leading-log generator ALPGEN [71] with the CTEQ6L1 [9] PDF and PYTHIA for parton showering. ALPGEN contains more tree-level graphs in higher-order α_s than PYTHIA. ALPGEN has parton-jet matching [72], which avoids double counting of partons in overlapping regions of jet kinematics. CDF sets the event generation factorization and renormalization scales Q^2 to $m_t^2 + p_\perp^2 + (P_1^2 + P_2^2)/2$, where $p_\perp$ is the transverse momentum characterizing the scattering process, and P_1^2 and P_2^2 are the virtualities of the incoming partons. D0 sets the scales to $m_t^2 + \langle p_T^2 \rangle$, where $\langle p_T^2 \rangle$ is the average of the square of transverse momentum of all other light partons produced in association with the $t\bar{t}$ pair. The PYTHIA model treats each step of the $t\bar{t}$ decay chain ($t{\rightarrow}Wb$, $W{\rightarrow}\ell\nu$ or $q\bar{q}'$) separately and does not preserve spin correlations. ALPGEN uses exact matrix elements for each step and thereby correctly describes the spin information of the final-state partons. The fragments of the proton and antiproton or "underlying event" are added separately to each hard collision. CDF uses the "Tune A" settings [73] in PYTHIA while D0 uses a modified version of the tune. Both collaborations use angular ordering for modeling parton showering in PYTHIA, and not p_T-ordered models. The underlying event is therefore not interleaved with the parton showers as in models of color reconnection [74].

D. Background models

In the lepton+jets channel, the dominant background is from W+jets production. Smaller contributions arise

from multijet events, Z+jets, single top-quark (tqb and tb), and diboson production (WW, WZ, and ZZ). The alljets channel has mainly multijet events as background. The largest background in the dilepton channel is from Z+jets events, which include Drell-Yan production. Backgrounds from diboson production and from events with jets identified as leptons are very small in the dilepton channel. The $\not{E}_T$+jets channel has multijet events and W+jets as main backgrounds.

In all channels contributions from multijet events are modeled using data. Most other background sources are modeled through MC simulation. In Run I, both collaborations used VECBOS [75] to model W+jets events. VECBOS is a precursor of ALPGEN and provides one of the first models of events with many high-momentum final-state partons. PYTHIA was used to model Z+jets, Drell-Yan, and diboson processes. Background from events with a single top quark was negligible. In Run II, both collaborations used ALPGEN for the simulation of the W+jets background. The treatment of heavy-flavor jets is implemented more accurately in ALPGEN, and parton-jet matching also improves the simulation. For the Z+jets background, CDF uses PYTHIA and D0 uses ALPGEN. For dibosons, both collaborations use PYTHIA. Processes with a single top quark are modeled by CDF using MADEVENT [76] (based on MADGRAPH [77]), and by D0 with SINGLETOP [78] (based on COMPHEP [79]).

The uncertainty in the description of the W+jets background has three main components: (i) the uncertainty on the scale Q^2, which affects both the overall normalization and the differential jet distributions in pseudorapidity η [80] and p_T; (ii) the uncertainty in the correction for flavor content of jets to higher order; and (iii) the limitation in the MC model we are using to reproduce the jet p_T and η distributions in data at low p_T and large $|\eta|$.

E. Jet properties

After the top quarks decay, the final-state quarks and gluons hadronize to produce multiple charged and neutral particles that traverse the central tracking systems into the calorimeters, where they produce many lower-momentum particles through interactions in the absorbers of the calorimeters. The observed particles tend to cluster in jets that can be assigned to the initial partons. For jet reconstruction, the CDF Collaboration uses a clustering algorithm in (η, ϕ) space [81] with a cone radius of

$$\text{CDF} \qquad \mathcal{R} = \sqrt{(\Delta\eta)^2 + (\Delta\phi)^2} = 0.4,$$

where ϕ is the azimuthal angle around the beamline, η is the pseudorapidity, and $\Delta\eta$ or $\Delta\phi$ are the widths of the cone. D0 uses a midpoint iterative seed-based cone algorithm in (y, ϕ) space [82] with a radius defined by

$$\text{D0} \qquad \mathcal{R} = \sqrt{(\Delta y)^2 + (\Delta\phi)^2} = 0.5,$$

where the rapidity $y = 1/2 \ln\left((E + p_L)/(E - p_L)\right)$, E is the jet energy, and p_L is its longitudinal momentum component.

The jet energy resolution in the central region ($|\eta| < 1$) is approximately the same for CDF and D0; for CDF it is $\sigma(E_T)/E_T = 50\%/\sqrt{E_T(GeV)} \oplus 3\%$. For jets in the forward region, however, the energy resolution at D0 is similar to that in the central region, while at CDF it is not as good [$\sigma(E_T)/E_T = 70\%/\sqrt{E_T(GeV)} \oplus 4\%$]. CDF's calorimeter covers $|\eta| < 3.8$ whereas D0's calorimeter covers $|\eta| < 4.2$. The D0 calorimeter is more homogeneous, so that the imbalance in transverse momentum (see Sec. II G) usually has better resolution at D0. For both CDF and D0, to reject jets with mismeasured energy, selections on energy deposition are required when clustering the energy from the calorimeter cells into jets. When a muon is reconstructed within the jet cone, a correction is applied to the jet energy to account for the muon and its associated neutrino assumed to arise from heavy-quark decay.

Jet energy scale calibrations are applied after jet reconstruction. CDF calibrates the transverse momentum using test-beam data and single-particle simulated events and corrects the jet energy to the parton level. Consequently, CDF does not calibrate the jet energy scale in MC events. D0 calibrates the energy using photon+jets and two-jet data and calibrates jets in data as well as in MC to the observed particle level. Particle jets are clustered from stable particles after fragmentation, including particles from the underlying event, but excluding undetected energy from muons and neutrinos.

CDF's jet calibration [83] applies two scale factors and three offsets to convert the measured transverse momentum of a jet to that of the parton that initiated the jet. D0's jet calibration [84] applies three scale factors and one offset to the jet energy to convert to the particle jet energy scale. The calibrations are expressed as follows:

$$\text{CDF} \qquad p_T^{\text{parton}} = \frac{p_T^{\text{jet}} \, R_{\text{rel}} - C_{\text{MI}}}{R_{\text{abs}}} - C_{\text{UE}} + C_{\text{OC}},$$

$$\text{D0} \qquad E^{\text{particle}} = \frac{E^{\text{jet}} - C_{\text{MI,UE}}}{R_{\text{abs}} \, R_{\text{rel}} \, F_{\text{OC}}}.$$

The absolute response R_{abs} corrects for energy lost in uninstrumented regions between calorimeter modules, for differences between electromagnetically and hadronically interacting particles, as well as for module-to-module irregularities. The relative response R_{rel} is a scale factor that corrects forward relative to central jets and C_{MI} is a correction for multiple interactions in the same bunch crossing. The function C_{UE} is a correction for the jet energy added from the underlying event. D0 has one offset correction, $C_{\text{MI,UE}}$, which includes the effects of multiple interactions, the underlying event, noise from radioactive decays of the uranium absorber, and the effect of collisions from previous bunch crossings (pileup). The functions C_{OC} and F_{OC} are corrections for shower particles scattered in or out of the cone of

radius $\mathcal{R}$. CDF's correction accounts for MC modeling that affects how the parton energy is translated into particle jet energy, whereas D0's correction accounts for a detector effect caused by the finite cell size in the calorimeter coupled with the cone size for the jet algorithm. The combined jet energy scale corrections increase the measured jet energies by about 20%–50%, depending on p_T and η.

The overall uncertainties on the jet energy scale corrections vary from about 2.7% for CDF and 1.1% for D0 for central jets of transverse energy of 100 GeV to 3.3% for CDF and 2.2% for D0 for forward jets. Central jets of 25 GeV have correction uncertainties of 5.9% for CDF and 1.4% for D0. For both experiments, the uncertainty on the corrections for absolute response $R_{\rm abs}$ dominate these uncertainties.

At D0, the jet energy resolution in data is inferior than predicted by the detector simulation. Therefore, the energies of MC jets are smeared so that the resulting resolution in MC matches that in data. Similarly, the reconstruction efficiency for jets in data is lower than is predicted by the detector simulation, so an appropriate fraction of MC jets are randomly removed. Both effects are corrected for as functions of jet p_T and pseudorapidity.

D0 Run II analyses include an energy correction to simulated jets that depends on jet flavor. There are corrections for b jets, other-quark flavor jets (u, d, s, and c), and gluon jets implemented in both the lepton+jets and dilepton analyses. Such corrections refine the simulation by improving the matching of jet energies in MC to data. The differences arise from the varying electromagnetic fractions and widths of the jets. The corrections depend on jet transverse energy and pseudorapidity and range from -6% to $+2\%$ [27].

Both collaborations perform an *in situ* jet energy scale calibration in lepton+jets events for the matrix-element mass extraction of m_t, and in CDF's alljets and $\displaystyle{\not}E_T$+jets measurements of m_t. The invariant mass of the two jets is constrained to a Breit-Wigner distribution for the $W \rightarrow q\bar{q}'$ decay, set to the world average value for the W-boson mass [7]. The energies of all jets in the event are then rescaled to complete this calibration.

F. *b*-quark jet properties

To separate top-quark events from background and to decrease the ambiguity in jet-to-parton matching, it is important to identify b-quark jets. Every $t\bar{t}$ event has two b jets, whereas such jets are rare in background. As B hadrons have a mean lifetime of $\approx 10^{-12}$ s, b jets can be tagged through secondary vertices of the B decay a few mm away from the primary $p\bar{p}$ interaction. CDF's b-tagging algorithm uses the significance of the displacement of the secondary vertex in the transverse (r, ϕ) plane for the lepton+jets and $\displaystyle{\not}E_T$+jets channels [59], as well as a jet-probability algorithm for $\displaystyle{\not}E_T$+jets events [63]. One parameter defines the significance of the separation of the primary and secondary

vertices for events with one and two b jets. For jets that are within the acceptance of the silicon microstrip tracker (i.e., "taggable" jets), this algorithm identifies 50% of real b jets and 9% of real charm jets, while falsely tagging 1% of light jets. D0 tags jets by combining nine track and secondary-vertex-related variables using a neural network [62]. For jets within the acceptance of the silicon microstrip detector, this yields efficiencies of 65% and 20% for real b and charm jets, respectively, while falsely tagging 3% of light jets.

To identify heavy-flavor jets in data and in MC events, the tagging algorithm is applied by CDF and D0 directly to the jets, except for simulated W+light jets events, where CDF uses tag-rate functions measured in multijet data, since the rate for directly-tagged MC events is very low. After applying direct tagging to b and c jets in MC events, D0 corrects the tagging efficiencies to match those observed in data by randomly dropping the tagging of 13% of such jets. For light-flavor jets, D0 assigns a per jet mistag weight.

G. Properties of other event observables

The uncertainty on m_t depends not only on an accurate measurement of jet energies and proper assignment of flavor, but also on the reconstruction and calibration of the other elements of the event, including electrons, muons, and the imbalance in transverse momentum, taking into account the presence of any simultaneous $p\bar{p}$ interactions in the same bunch crossing.

The mean number of $p\bar{p}$ collisions per bunch crossing is ≈ 2 in Run I and ≈ 5 in Run II. Such additional collisions affect the observed characteristics of the hard scatter of interest and must be included in the MC simulation. These extra collisions result mostly in the production of low-p_T particles. CDF simulates such additional interactions using the PYTHIA model of minimum-bias events and overlays them onto the hard scatters using a Poisson mean appropriate to the instantaneous luminosity of the data. In a similar manner D0 overlays randomly triggered data events with the same luminosity profile as the data onto the MC simulated events.

Electrons are identified by matching clusters of energy deposited in the electromagnetic layers of the calorimeters with tracks that point from the primary collision vertex to the clusters. The spatial shapes of the showers must agree with those expected for electrons, as studied in test-beam data. The energy of an electron is determined as a combination of the total energy of the cluster and the momentum measured from the curvature of the matching track. The reconstruction efficiency is determined using $Z \rightarrow ee$ data by identifying one tight charged lepton a as tag and using the other charged lepton as a probe (tag-and-probe method). The electron energy is also recalibrated using such Z events.

Muons are reconstructed from a central track and matched to a track in the outer muon chambers. In D0, both the inner and outer trajectories pass through

magnetic fields, and so the transverse momenta of the two are therefore required to match. The reconstruction efficiency and calibration of p_T are determined using a tag-and-probe method applied on $J/\psi \rightarrow \mu\mu$ and $Z \rightarrow \mu\mu$ events in a manner similar to that used for electrons.

As indicated above, all $t\bar{t}$ decay channels except for alljets events have a large $\not{E}_T$. All jet energy calibration corrections are also propagated to $\not{E}_T$ in each event.

III. COMBINATION OF MASS MEASUREMENTS

A. BLUE combination method

The basic idea of the technique, called the best linear unbiased estimator (BLUE) method [34–36], used to obtain the combined mass m_t^{comb}, an "estimator" of the true mass m_t^{true}, is to calculate a linear weighted sum of the results from separate measurements:

$$m_t^{\text{comb}} = \sum_{i=1}^{12} w_i \, m_t^i. \tag{1}$$

The m_t^i are the 12 CDF and D0 measurements i of m_t and

$$\sum_{i=1}^{12} w_i = 1. \tag{2}$$

The weights are determined using the value of m_t^{comb} that minimizes the squared difference relative to the unknown true value m_t^{true}:

$$\left(m_t^{\text{comb}} - m_t^{\text{true}}\right)^2 =$$
$$\text{Variance}\left(m_t^{\text{comb}}\right) + \left[\text{Bias}\left(m_t^{\text{comb}}\right)\right]^2, \tag{3}$$

where the two terms represent the weighted variance and bias in the 12 input m_t values with

$$\text{Variance}\left(m_t^{\text{comb}}\right) = \sum_{i=1}^{12} w_i^2 \, \text{Variance}\left(m_t^i\right), \tag{4}$$

and

$$\text{Variance}\left(m_t^i\right) = \left[\sigma\left(m_t^i\right)\right]^2, \tag{5}$$

where $\sigma\left(m_t^i\right)$ are the uncertainties on the 12 input values given in Table I.

On average, we expect the input mass measurements to be unbiased, and we therefore assume

$$\text{Bias}\left(m_t^{\text{comb}}\right) = \sum_{i=1}^{12} w_i \, \text{Bias}\left(m_t^i\right) = 0. \tag{6}$$

Equation (3) shows that the BLUE method defines the best estimate through a minimization of the variance of m_t for an assumed unbiased set of measurements. The minimum corresponds to setting the weights to

$$w_i = \frac{1/\text{Variance}\left(m_t^i\right)}{\sum_{i=1}^{12} 1/\text{Variance}\left(m_t^i\right)} \tag{7}$$

for uncorrelated input values. Since the input m_t values are correlated, the variance in Eq. (4) has to be replaced with a covariance matrix:

$$\text{Variance}\left(m_t^{\text{comb}}\right) =$$
$$\sum_{i=1}^{12} \sum_{j=1}^{12} w_i \, w_j \, \text{Covariance}\left(m_t^i, m_t^j\right), \tag{8}$$

which is defined as

$$\text{Covariance}\left(m_t^i, m_t^j\right) =$$
$$\left[\sigma\left(m_t^i \, m_t^j\right)\right]^2 - \sigma\left(m_t^i\right)\sigma\left(m_t^j\right). \tag{9}$$

Minimizing Eq. (3) yields

$$w_i = \frac{\sum_{j=1}^{12} \text{Covariance}^{-1}\left(m_t^i, m_t^j\right)}{\sum_{i=1}^{12} \sum_{j=1}^{12} \text{Covariance}^{-1}\left(m_t^i, m_t^j\right)}, \tag{10}$$

where $\text{Covariance}^{-1}\left(m_t^i, m_t^j\right)$ are the elements of the inverse of the covariance matrix (also known as the error matrix), and

$$\text{Covariance}\left(m_t^i, m_t^j\right) =$$
$$\text{Correlation}\left(m_t^i, m_t^j\right) \sigma\left(m_t^i\right)\sigma\left(m_t^j\right) \tag{11}$$

with $\text{Correlation}\left(m_t^i, m_t^j\right)$ the correlation coefficient between m_t^i and m_t^j. The following sections show how the correlation matrix is derived by examining the uncertainty components and their individual correlations.

B. Measurement uncertainties

The uncertainty on any m_t measurement has a statistical component from the limited number of events available for the measurement and a systematic component from the uncertainties assigned to the calibration of input quantities, to the model of the signal, and to the calibration of the mass extraction method. Since the first measurements of m_t [4, 5], the systematic component has been slightly larger than the statistical one. As more data became available, the statistical uncertainties on m_t improved as did the calibrations of systematic uncertainty, and the two components therefore improved together.

The systematic uncertainty on each m_t measurement in this combination is divided into 14 parts. Some of them have origin in only one source whereas, others include several related sources of uncertainties. For the latter the patterns of correlation among different channels, Tevatron Run I and Run II, or experiments are the same for all sources included in these systematic components. The uncertainty on jet energy scale (JES), on the other hand, is split into seven components, which do not appply to all measurements, given the significantly different approaches to jet energy calibration between CDF and D0 and the change in the D0 procedure between Run I and Run II.

Table II gives the uncertainty of each of the 12 top-quark mass measurements for the different contributions to uncertainty and their effect on the final combination. The components of uncertainty are defined in the following and can be classified as uncertainties in detector response (jet energy scale, jet and lepton modeling), uncertainties from modeling signal and background (signal modeling, multiple interactions model, background estimated from theory, and background based on data), uncertainties from method of mass extraction, and statistical uncertainties. A detailed description of the methods to evaluate these systematic uncertainties is presented in the Appendix.

1. Jet energy scale

1.1 Light-jet response (1)

One subcomponent of the uncertainty in JES covers the absolute calibration for CDF's Run I and Run II measurements. It also includes small contributions from the uncertainties associated with modeling multiple interactions within a single bunch crossing and corrections for the underlying event.

1.2 Light-jet response (2)

Another subcomponent of this uncertainty includes D0's Run I and Run II calibrations of absolute response (energy dependent), the relative response (η dependent), and the out-of-cone showering correction that is a detector effect. This uncertainty term for CDF includes only the small relative response calibration (η dependent) for Run I and Run II.

1.3 Out-of-cone correction

This subcomponent of the JES uncertainty quantifies the out-of-cone showering corrections to the MC showers for all of CDF's and for D0's Run I measurements that are obtained by varying the model for light-quark fragmentation.

1.4 Offset

This subcomponent originates from the offset in D0's Run I calibration, which corrects for noise from uranium decay, pileup from previous collisions, and for multiple interactions and the model for the underlying event. In Run I, the uncertainties are large, but in Run II, owing to the smaller integration time for calorimeter electronics, they are negligible. CDF's calorimeter does not have the

same sources of noise and sensitivity to pileup as D0, so CDF measurements do not have this term.

1.5 Model for b jets

This subcomponent comes from the uncertainty on the semileptonic branching fraction in b decays and from differences between two models of b-jet hadronization.

1.6 Response to $b/q/g$ jets

This subcomponent accounts for the difference in the electromagnetic versus hadronic response of b jets, light-quark jets, and gluon jets. CDF corrects for jet flavor as part of the main calibration, and defines the uncertainty based on the remaining difference in response between b jets and light-flavor jets, whereas D0 corrects the response for b, light-quark (u, d, s, and c), and gluon jets as a function of jet p_T and η.

1.7 *In situ* light-jet calibration

The last part of the uncertainty in the jet energy scale is from the *in situ* calibration of m_t. It corresponds to the statistical uncertainty from the limited number of events used in the fit when using the W-boson mass to constrain the energies of the light quarks from the W decay.

2. Jet modeling

The uncertainty in jet modeling has two components for D0. This uncertainty is negligible for CDF.
(i) The jet energy resolution is smeared for MC jets to match the resolution observed in data, and the uncertainty on the smearing functions is propagated to m_t.
(ii) The identification efficiency in MC events is corrected to match that found in data, and the uncertainty on the correction functions is propagated to m_t.

3. Lepton modeling

This uncertainty has two components:
(i) The electron and muon p_T scales are calibrated to the J/ψ and Z-boson mass by both CDF and D0. This uncertainty on the calibration is included in the measurements of m_t.
(ii) D0 smears the muon momentum resolution in MC events to match that in data, and the uncertainty on this correction is included in this term. The uncertainty on the electron resolution has a negligible impact on the measurements of m_t.

4. Signal modeling

There are six components to this uncertainty. They are combined into one term because the correlations between channels are similar for each component:
(i) Knowledge of the PDF parametrization.
(ii) The quark annihilation and gluon fusion fractions that differ significantly between leading-log and next-to-leading-order (NLO) QCD calculations (Run II).
(iii) The amount of initial- and final-state radiation in MC signal events differs from that in data and is adjusted through the value of Λ_{QCD} used in the shower and the scales of time and spacelike showers.

TABLE II: The uncertainty in GeV from each component for the 12 measurements of m_t and the resulting Tevatron combination. The total uncertainties are obtained by adding the components in quadrature. The entries "n/a" stand for "not applicable" and "n/e" for "not evaluated." The nonevaluated uncertainties were not considered as significant sources of uncertainty for Run I measurements.

Channel	Run	Exp.	Light-jet response (1)	Light-jet response (2)	Out-of-cone correction	Offset	Model for b jets	Response to $b/q/g$ jets	In situ light-jet calibration	Jet modeling	Lepton modeling	Signal modeling	Multiple interactions model	Background from theory	Background based on data	Calibration method	Statistical uncertainty	Total JES uncertainty	Other systematic uncertainty	Total uncertainty
			Jet energy scale systematics							Other systematics										
Lepton+jets	II	CDF	0.41	0.01	0.27	n/a	0.23	0.13	0.58	0.00	0.14	0.56	0.10	0.27	0.06	0.10	0.65	0.80	0.67	1.23
Lepton+jets	II	D0	n/a	0.63	n/a	n/a	0.07	0.26	0.46	0.36	0.18	0.77	0.05	0.19	0.23	0.16	0.83	0.83	0.94	1.50
Lepton+jets	I	CDF	3.4	0.7	2.7	n/a	0.6	n/e	n/a	n/e	n/e	2.7	n/e	1.3	n/e	0.0	5.1	4.4	2.8	7.3
Lepton+jets	I	D0	n/a	2.5	2.0	1.3	0.7	n/e	n/a	n/e	n/e	1.3	n/e	1.0	n/e	0.6	3.6	3.5	1.6	5.3
Alljets	II	CDF	0.38	0.04	0.24	n/a	0.15	0.03	0.95	0.00	n/a	0.64	0.08	0.00	0.56	0.38	1.43	1.06	0.91	2.00
Alljets	I	CDF	4.0	0.3	3.0	n/a	0.6	n/e	n/a	n/e	n/a	2.1	n/e	1.7	n/e	0.6	10.0	5.0	2.6	11.5
Dileptons	II	CDF	2.01	0.58	2.13	n/a	0.33	0.14	n/a	0.00	0.27	0.80	0.23	0.24	0.14	0.12	1.95	3.01	0.88	3.69
Dileptons	II	D0	n/a	0.56	n/a	n/a	0.20	0.40	0.55	0.50	0.35	0.86	0.00	0.00	0.20	0.51	2.36	0.90	1.11	2.76
Dileptons	I	CDF	2.7	0.6	2.6	n/a	0.8	n/e	n/a	n/e	n/e	3.0	n/e	0.3	n/e	0.0	10.3	3.9	3.0	11.4
Dileptons	I	D0	n/a	1.1	2.0	1.3	0.7	n/e	n/a	n/e	n/e	1.9	n/e	1.1	n/e	1.1	12.3	2.7	2.3	12.8
E_T+jets	II	CDF	0.45	0.05	0.20	n/a	0.00	0.12	1.54	0.00	n/a	0.78	0.16	0.00	0.12	0.14	1.80	1.64	0.78	2.56
Decay length	II	CDF	0.24	0.06	n/a	n/a	0.15	n/e	n/a	0.00	n/a	0.90	0.00	0.80	0.20	2.50	9.00	0.25	2.80	9.43
Tevatron combination			0.12	0.19	0.04	0.00	0.15	0.12	0.39	0.11	0.10	0.51	0.00	0.14	0.11	0.09	0.56	0.49	0.57	0.94

(iv) Higher-order QCD corrections to initial- and final-state radiation differ from precise parton-level models, and this is not accounted for by the choice of scale for the calculations (Run II).

(v) Our model for jet hadronization is based on angular ordering in PYTHIA with Tune A underlying-event tuning. Parton showering and the underlying event can also be simulated with HERWIG and JIMMY [85, 86]. The effect of the difference on m_t between the two models is included in this term.

(vi) Final-state partons and remnants of the protons and antiprotons are connected through color strings, which affect the distributions of jets. Since this effect is not included in the model for the $t\bar{t}$ signal, the value of m_t has an uncertainty from this omission (Run II).

5. Multiple interactions model

The number of soft $p\bar{p}$ events overlaid on each MC event has a Poisson distribution. The mean number does not equal exactly the number seen in data since the luminosity increased as the Tevatron run progressed. The top-quark mass is measured as a function of the number of multiple interactions in signal events by CDF, the signal MC events are reweighted to match the distribution seen in data by D0, and the related uncertainties are included here.

6. Background from theory

There are four components in this uncertainty:

(i) Difference between NLO calculations of the fraction of heavy-flavor jets in W+jets events. The ALPGEN model underestimates this fraction.

(ii) Impact of factorization and renormalization scales on the W+jets simulation, which affects the background model for distributions characterizing jets.

(iii) The theoretical cross sections used to normalize all MC estimated background processes (except for W+jets for CDF and D0 lepton+jets measurements, and Drell-Yan production for CDF dilepton measurements).

(iv) Impact of difference between the MC modeling of background kinematic distributions and those observed in data.

7. Background based on data

This refers primarily to uncertainties from the normalization of certain background components to data. These include multijet backgrounds in the lepton+jets, alljets, and E_T+jets analyses, the W+jets background in the D0 lepton+jets analyses, and the Drell-Yan backgrounds in the CDF dilepton analyses.

D0 also considers the following four components of uncertainty:

(i) The uncertainty from correcting the MC events to match the trigger efficiency in data, which is based on the turn-on response for each trigger element.

(ii) The uncertainty from applying tag-rate and taggability corrections to MC events to make the efficiencies match the data for each jet flavor.

TABLE III: Correlations in systematic uncertainties (in percent) among the different measurements of m_t.

			Lepton+jets Run II CDF	Lepton+jets Run II D0	Lepton+jets Run I CDF	Lepton+jets Run I D0	Alljets Run II CDF	Alljets Run I CDF	Dileptons Run II CDF	Dileptons Run II D0	Dileptons Run I CDF	Dileptons Run I D0	$\not{E}_T$+jets Run II CDF	Decay length Run II CDF
			Calibration method					Statistical uncertainty						
			Not correlated among any measurements											
			In situ light-jet calibration (JES)											
Lepton+jets	Run II	CDF	100	0	0	0	0	0	0	0	0	0	0	0
Lepton+jets	Run II	D0	0	100	0	0	0	0	0	100	0	0	0	0
Lepton+jets	Run I	CDF	0	0	100	0	0	0	0	0	0	0	0	0
Lepton+jets	Run I	D0	0	0	0	100	0	0	0	0	0	0	0	0
Alljets	Run II	CDF	0	0	0	0	100	0	0	0	0	0	0	0
Alljets	Run I	CDF	0	0	0	0	0	100	0	0	0	0	0	0
Dileptons	Run II	CDF	0	0	0	0	0	0	100	0	0	0	0	0
Dileptons	Run II	D0	0	100	0	0	0	0	0	100	0	0	0	0
Dileptons	Run I	CDF	0	0	0	0	0	0	0	0	100	0	0	0
Dileptons	Run I	D0	0	0	0	0	0	0	0	0	0	100	0	0
$\not{E}_T$+jets	Run II	CDF	0	0	0	0	0	0	0	0	0	0	100	0
Decay length	Run II	CDF	0	0	0	0	0	0	0	0	0	0	0	100
			Background based on data											
Lepton+jets	Run II	CDF	100	0	0	0	0	0	0	0	0	0	0	100
Lepton+jets	Run II	D0	0	100	0	0	0	0	0	0	0	0	0	0
Lepton+jets	Run I	CDF	0	0	100	0	0	0	0	0	0	0	0	0
Lepton+jets	Run I	D0	0	0	0	100	0	0	0	0	0	0	0	0
Alljets	Run II	CDF	0	0	0	0	100	0	0	0	0	0	0	0
Alljets	Run I	CDF	0	0	0	0	0	100	0	0	0	0	0	0
Dileptons	Run II	CDF	0	0	0	0	0	0	100	0	0	0	0	0
Dileptons	Run II	D0	0	0	0	0	0	0	0	100	0	0	0	0
Dileptons	Run I	CDF	0	0	0	0	0	0	0	0	100	0	0	0
Dileptons	Run I	D0	0	0	0	0	0	0	0	0	0	100	0	0
$\not{E}_T$+jets	Run II	CDF	0	0	0	0	0	0	0	0	0	0	100	0
Decay length	Run II	CDF	100	0	0	0	0	0	0	0	0	0	0	100
			Background from theory											
Lepton+jets	Run II	CDF	100	100	100	100	0	0	0	0	0	0	0	100
Lepton+jets	Run II	D0	100	100	100	100	0	0	0	0	0	0	0	100
Lepton+jets	Run I	CDF	100	100	100	100	0	0	0	0	0	0	0	100
Lepton+jets	Run I	D0	100	100	100	100	0	0	0	0	0	0	0	100
Alljets	Run II	CDF	0	0	0	0	100	100	0	0	0	0	0	0
Alljets	Run I	CDF	0	0	0	0	100	100	0	0	0	0	0	0
Dileptons	Run II	CDF	0	0	0	0	0	0	100	100	100	100	0	0
Dileptons	Run II	D0	0	0	0	0	0	0	100	100	100	100	0	0
Dileptons	Run I	CDF	0	0	0	0	0	0	100	100	100	100	0	0
Dileptons	Run I	D0	0	0	0	0	0	0	100	100	100	100	0	0
$\not{E}_T$+jets	Run II	CDF	0	0	0	0	0	0	0	0	0	0	100	0
Decay length	Run II	CDF	100	100	100	100	0	0	0	0	0	0	0	100
			Light-jet response (2) (JES)				Offset (JES)		Response to $b/q/g$ jets (JES)					
			Jet modeling				Lepton modeling		Multiple interactions model					
Lepton+jets	Run II	CDF	100	0	0	0	100	0	100	0	0	0	100	100
Lepton+jets	Run II	D0	0	100	0	0	0	0	0	100	0	0	0	0
Lepton+jets	Run I	CDF	0	0	100	0	0	100	0	0	100	0	0	0
Lepton+jets	Run I	D0	0	0	0	100	0	0	0	0	0	100	0	0
Alljets	Run II	CDF	100	0	0	0	100	0	100	0	0	0	100	100
Alljets	Run I	CDF	0	0	100	0	0	100	0	0	100	0	0	0
Dileptons	Run II	CDF	100	0	0	0	100	0	100	0	0	0	100	100
Dileptons	Run II	D0	0	100	0	0	0	0	0	100	0	0	0	0
Dileptons	Run I	CDF	0	0	100	0	0	100	0	0	100	0	0	0
Dileptons	Run I	D0	0	0	0	100	0	0	0	0	0	100	0	0
$\not{E}_T$+jets	Run II	CDF	100	0	0	0	100	0	100	0	0	0	100	100
Decay length	Run II	CDF	100	0	0	0	100	0	100	0	0	0	100	100

TABLE IV: Correlations in systematic uncertainties (in percent) among the different measurements of m_t (continued).

			Lepton+jets Run II CDF	Lepton+jets Run II D0	Lepton+jets Run I CDF	Lepton+jets Run I D0	Alljets Run II CDF	Alljets Run I CDF	Dileptons Run II CDF	Dileptons Run II D0	Dileptons Run I CDF	Dileptons Run I D0	$\not{E}_T$+jets Run II CDF	Decay length Run II CDF
			Light-jet response (1) (JES)											
Lepton+jets	Run II	CDF	100	0	100	0	100	100	100	0	100	0	100	100
Lepton+jets	Run II	D0	0	100	0	100	0	0	0	100	0	100	0	0
Lepton+jets	Run I	CDF	100	0	100	0	100	100	100	0	100	0	100	100
Lepton+jets	Run I	D0	0	100	0	100	0	0	0	100	0	100	0	0
Alljets	Run II	CDF	100	0	100	0	100	100	100	0	100	0	100	100
Alljets	Run I	CDF	100	0	100	0	100	100	100	0	100	0	100	100
Dileptons	Run II	CDF	100	0	100	0	100	100	100	0	100	0	100	100
Dileptons	Run II	D0	0	100	0	100	0	0	0	100	0	100	0	0
Dileptons	Run I	CDF	100	0	100	0	100	100	100	0	100	0	100	100
Dileptons	Run I	D0	0	100	0	100	0	0	0	100	0	100	0	0
$\not{E}_T$+jets	Run II	CDF	100	0	100	0	100	100	100	0	100	0	100	100
Decay length	Run II	CDF	100	0	100	0	100	100	100	0	100	0	100	100

Out-of-cone correction (JES)   Model for b jets (JES)   Signal modeling

100% correlated among all measurements

(iii) The uncertainty on the fraction of multijet events included in the pseudoexperiments used for calibration.

8. Calibration method

The extracted values of m_t are calibrated using a straight-line fit to the relationship between input mass and measured mass in simulated pseudoexperiments. This term includes the systematic uncertainties from the slope and offset of this calibration.

9. Statistical uncertainty

The statistical uncertainties are determined from the number of data events in each of the 12 measurements.

Figure 5 shows the relative contribution for each major uncertainty to the analysis channels in Run II. The Appendix provides more detail on how each of the sources of the uncertainties is estimated.
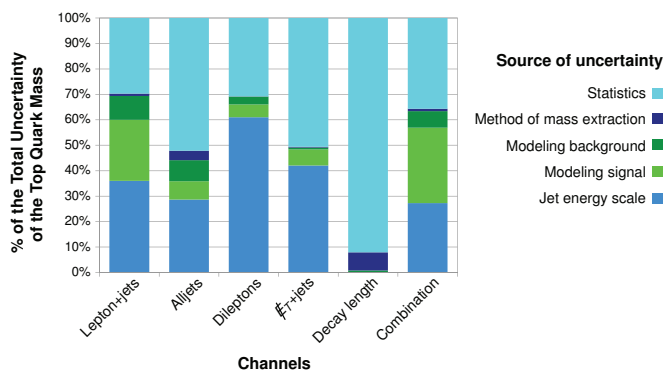

FIG. 5: The average uncertainties for CDF and D0 for each Run II measurement and for the Tevatron combination, separated according to major components. (See Table VIII in the Appendix for details on the systematic categories. In this figure, the jet and lepton modeling systematic uncertainties are grouped into the modeling background category.)

C. Uncertainty correlations

Tables III and IV indicate how uncertainties are correlated between measurements. There are seven patterns of correlation:

(i) Statistical uncertainty and calibration method uncertainty are not correlated among the measurements.
(ii) Correlations among D0 measurements that implement the same final jet energy corrections for the uncertainty from *in situ* light-jet calibration.
(iii) Correlations among CDF measurements that use the same data samples for the uncertainty from background based on data.
(iv) Correlations among all measurements in the same $t\bar{t}$ decay channel for the uncertainty from background estimated from theory.

(v) Correlations of measurements within the same experiment for a given run period for the uncertainties from light-jet response (2), offset, response to $b/q/g$ jets, jet modeling, lepton modeling and multiple interactions model.
(vi) Correlations for measurements within the same experiment such as the uncertainty from light-jet response (1).
(vii) Correlations among all measurements such as the uncertainties from out-of-cone correction, model for b jets, and signal modeling.

We assume that all sources correspond to either no or 100% correlation. A check of this assumption (see Sec. IV B) shows that it has a negligible effect on the combined value and uncertainty of m_t.

D. Measurement correlations

The uncertainties shown in Table II and their correlations shown in Tables III and IV provide the correlations among the 12 input values of m_t. The correlation matrix for these measurements, as returned by the combination procedure, is shown in Table V. The inversion of the covariance matrix built with the correlation matrix defines the measurement weights, as described in Sec. III A.

E. Measurement weights

As discussed in Sec. III A, the combined mass m_t^{comb} is defined through the set of weights that minimize the squared difference between m_t^{comb} and the true value of m_t, which is equivalent to minimizing the sum of the covariance matrix elements. Table V gives the weights w_i for each of the input measurements as determined in this minimization. A weight of zero means that an input measurement has no effect on m_t^{comb}. The Run I measurement weights are negative, which reflects the fact that the correlations for these and other measurements are larger than the ratio of their total uncertainties [35]. In this case, the less precise measurement may acquire a negative weight. Input measurements with negative weights still affect the value of m_t^{comb} and reduce the total uncertainty. By design, the sum of the weights is set to unity.

IV. RESULTS OF THE COMBINATION

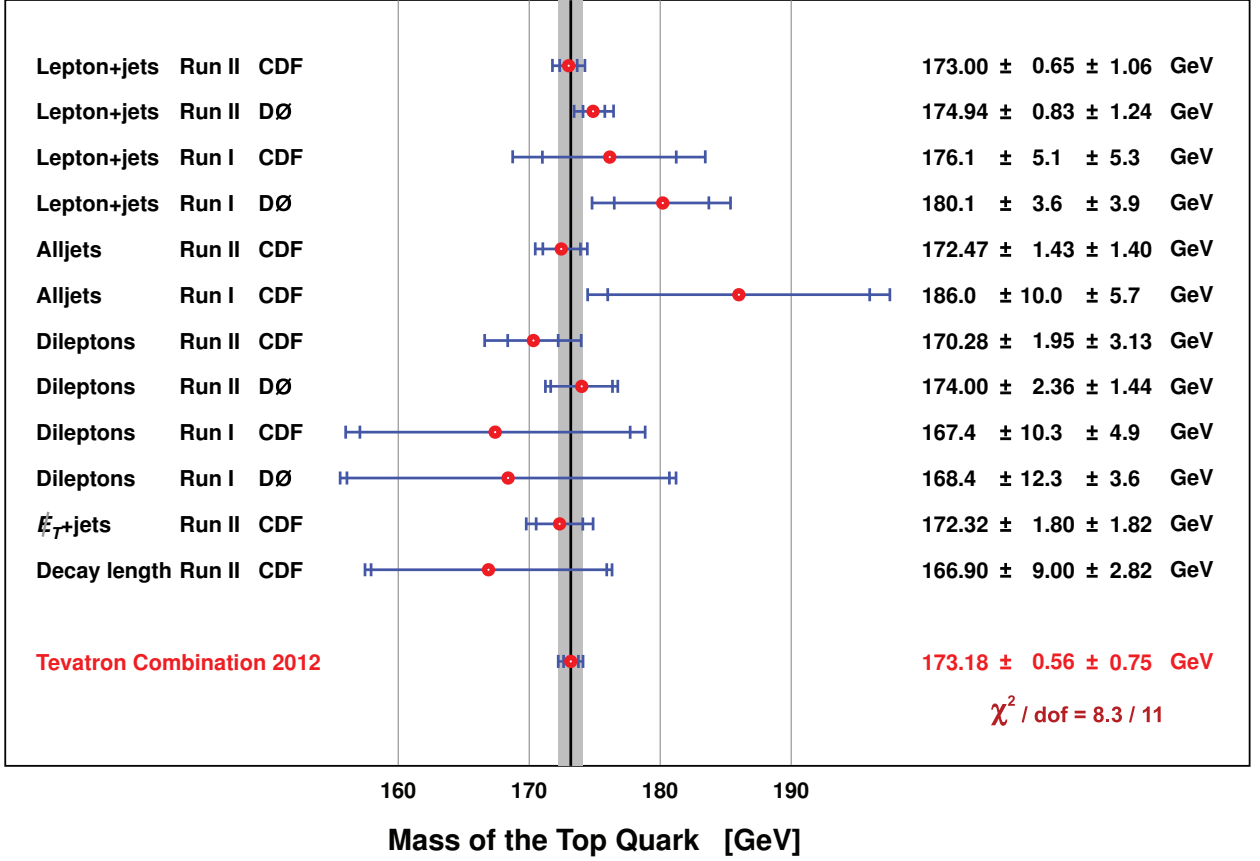### A. Tevatron top-quark mass result

Combining the 12 independent measurements of m_t from the CDF and D0 Collaborations yields

$$m_t^{\mathrm{comb}} = 173.18 \pm 0.56\,(\mathrm{stat}) \pm 0.75\,(\mathrm{syst})\ \mathrm{GeV}$$
$$= 173.18 \pm 0.94\ \mathrm{GeV}.$$

The uncertainties are split into their components in Table II and Fig. 5. The jet energy scale contributes

TABLE V: Correlations in % among the input m_t measurements and their weights in the BLUE combination.

			Lepton+jets Run II CDF	Lepton+jets Run II D0	Lepton+jets Run I CDF	Lepton+jets Run I D0	Alljets Run II CDF	Alljets Run I CDF	Dileptons Run II CDF	Dileptons Run II D0	Dileptons Run I CDF	Dileptons Run I D0	$\not{E}_T$+jets Run II CDF	Decay length Run II CDF	Weight
Lepton+jets	Run II	CDF	100	27	45	25	25	26	44	12	26	11	24	8	55.50
Lepton+jets	Run II	D0	27	100	21	14	16	9	11	39	13	7	15	6	26.66
Lepton+jets	Run I	CDF	45	21	100	26	25	32	54	12	29	11	22	7	-4.72
Lepton+jets	Run I	D0	25	14	26	100	12	14	27	7	15	16	10	5	-0.06
Alljets	Run II	CDF	25	16	25	12	100	15	25	10	15	7	14	4	13.99
Alljets	Run I	CDF	26	9	32	14	15	100	38	6	19	7	14	4	-0.80
Dileptons	Run II	CDF	44	11	54	27	25	38	100	7	32	13	22	6	1.41
Dileptons	Run II	D0	12	39	12	7	10	6	7	100	8	5	10	3	2.28
Dileptons	Run I	CDF	26	13	29	15	15	19	32	8	100	8	14	4	-1.05
Dileptons	Run I	D0	11	7	11	16	7	7	13	5	8	100	6	2	-0.15
$\not{E}_T$+jets	Run II	CDF	24	15	22	10	14	14	22	10	14	6	100	4	6.65
Decay length	Run II	CDF	8	6	7	5	4	4	6	3	4	2	4	100	0.29

Lepton+jets	**Run II**	**CDF**	173.00 ± 0.65 ± 1.06 GeV
Lepton+jets	**Run II**	**DØ**	174.94 ± 0.83 ± 1.24 GeV
Lepton+jets	**Run I**	**CDF**	176.1 ± 5.1 ± 5.3 GeV
Lepton+jets	**Run I**	**DØ**	180.1 ± 3.6 ± 3.9 GeV
Alljets	**Run II**	**CDF**	172.47 ± 1.43 ± 1.40 GeV
Alljets	**Run I**	**CDF**	186.0 ± 10.0 ± 5.7 GeV
Dileptons	**Run II**	**CDF**	170.28 ± 1.95 ± 3.13 GeV
Dileptons	**Run II**	**DØ**	174.00 ± 2.36 ± 1.44 GeV
Dileptons	**Run I**	**CDF**	167.4 ± 10.3 ± 4.9 GeV
Dileptons	**Run I**	**DØ**	168.4 ± 12.3 ± 3.6 GeV
$\not{E}_T$+jets	**Run II**	**CDF**	172.32 ± 1.80 ± 1.82 GeV
Decay length	**Run II**	**CDF**	166.90 ± 9.00 ± 2.82 GeV
Tevatron Combination 2012			**173.18 ± 0.56 ± 0.75 GeV**

χ^2 / dof = 8.3 / 11

Mass of the Top Quark [GeV]

FIG. 6: The 12 input measurements of m_t from the Tevatron collider experiments along with the resulting combined value of m_t^{comb}. The gray region corresponds to ± 0.94 GeV.

0.49 GeV to the total systematic uncertainty. Of this, 0.39 GeV arises from limited statistics of the *in situ* JES calibration and 0.30 GeV from the remaining contributions. Figure 6 summarizes the input m_t values and the combined result.

We assess the consistency of the input m_t measurements with their combination using a χ^2

TABLE VI: Separate calculations of m_t^{comb} for each $t\bar{t}$ decay mode, by run period, and by experiment, and their χ^2 probabilities.

Subset	m_t^{comb}	Consistency χ^2 (Degrees of freedom = 1)						χ^2 probability					
		Lepton+jets	Alljets	Dileptons	$\not{E}_T$+jets	Run II – Run I	CDF – D0	Lepton+jets	Alljets	Dileptons	$\not{E}_T$+jets	Run II – Run I	CDF – D0
Lepton+jets	173.4 ± 1.0	—	0.14	1.51	0.28			—	71%	22%	60%		
Alljets	172.7 ± 1.9	0.14	—	0.40	0.04			71%	—	53%	85%		
Dileptons	171.1 ± 2.1	1.51	0.40	—	0.12			22%	53%	—	73%		
$\not{E}_T$+jets	172.1 ± 2.5	0.28	0.04	0.12	—			60%	85%	73%	—		
Run II	173.6 ± 1.0					2.89						9%	
Run I	180.0 ± 4.1					2.89						9%	
CDF	172.5 ± 1.0						2.56						11%
D0	174.9 ± 1.4						2.56						11%

test statistic, defined as follows:

$$\chi^2_{\mathrm{comb}} = \left(\boldsymbol{m_t^i} - \boldsymbol{m_t^{\mathrm{comb}}}\right)^T$$
$$\times \, \mathrm{Covariance}^{-1}\left(m_t^i, m_t^j\right)\left(\boldsymbol{m_t^j} - \boldsymbol{m_t^{\mathrm{comb}}}\right),$$

where $\boldsymbol{m_t^i}$ is a column vector of the 12 m_t inputs, $\boldsymbol{m_t^{\mathrm{comb}}}$ is a matching column vector for the measurements adjusted in the previous minimization, and the superscript T denotes the transpose. We find

$$\chi^2_{\mathrm{comb}} = 8.3 \text{ for 11 degrees of freedom,}$$

which is equivalent to a 69% probability for agreement (i.e., p value for the observed χ^2 value) among the 12 input measurements.

B. Consistency checks

We check one aspect of the assumption that biases in the input m_t are on average zero (see Sec. III A) by calculating separately the combined m_t^{comb} for each $t\bar{t}$ decay mode, each run period, and each experiment. The results are shown in Table VI. The resulting m_t^{comb} values are calculated using all 12 input measurements and their correlations. The χ^2 test statistic provides the compatibility of each subset with the others and is defined as

$$\chi^2_{\mathrm{sub1,sub2}} =$$
$$\left(m_t^{\mathrm{sub1}} - m_t^{\mathrm{sub2}}\right)^2 \mathrm{Covariance}^{-1}\left(m_t^{\mathrm{sub1}}, m_t^{\mathrm{sub2}}\right).$$

The χ^2 values in Table VI show that biases in the input measurements are not large.

To check the impact of the assumption that the systematic uncertainty terms are either 0% or 100% correlated between input measurements, we change all off-diagonal 100% values to 50% (see Tables III and IV) and recalculate the combined top-quark mass. This

extreme change shifts the central mass value up by 0.17 GeV and reduces the uncertainty negligibly. The chosen approach is therefore conservative.

C. Summary

We have combined 12 measurements of the mass of the top quark by the CDF and D0 collaborations at the Tevatron collider and find

$$m_t^{\mathrm{comb}} = 173.18 \pm 0.56 \,(\mathrm{stat}) \pm 0.75 \,(\mathrm{syst}) \text{ GeV}$$

which corresponds to a precision of 0.54%. The result is shown in Table VII together with previous combined results for comparison. The input measurements for this combination use up to 5.8 fb^{-1} of integrated luminosity for each experiment, while 10 fb^{-1} are now available. We therefore expect the final combination to improve in precision with the use of all the data, but also from analyzing all $t\bar{t}$ decay channels in both experiments, and from the application of improved measurement techniques, signal and background models, and calibration corrections to all channels that will reduce systematic uncertainties. Currently, there are also some overlaps of the systematic effects that are included in different uncertainty categories. In addition to the *in situ* light-jet calibration systematic uncertainty that will scale down with the increase of analyzed luminosity, these levels of double counting are expected to be reduced for the next combination. The combination presented here has a 0.54% precision on m_t, making the top quark the particle with the best known mass in the SM.

TABLE VII: Mass measurements of the top quark from 1999 until this publication at the Tevatron collider.

Year	Integrated luminosity [fb^{-1}]	m_t [GeV]			Uncertainty on m_t	Reference
1999	0.1	174.3	± 3.2	± 4.0	2.9%	[37]
2004	0.1	178.0	± 2.7	± 3.3	2.4%	[38]
2005	0.3	172.7	± 1.7	± 2.4	1.7%	[39]
2006	0.7	172.5	± 1.3	± 1.9	1.3%	[40]
2006	1.0	171.4	± 1.2	± 1.8	1.2%	[41]
2007	2.1	170.9	± 1.1	± 1.5	1.1%	[42]
2008	2.1	172.6	± 0.8	± 1.1	0.8%	[43]
2008	2.1	172.4	± 0.7	± 1.0	0.7%	[44]
2009	3.6	173.1	± 0.6	± 1.1	0.7%	[45]
2010	5.6	173.32	± 0.56	± 0.89	0.61%	[46]
2011	5.8	173.18	± 0.56	± 0.75	0.54%	[47]
	5.8	173.18	± 0.56	± 0.75	0.54%	This paper

FAPESP and FUNDUNESP (Brazil), NSERC (Canada), NSC, CAS and CNSF (China), Colciencias (Colombia), MSMT and GACR (Czech Republic), the Academy of Finland, CEA and CNRS/IN2P3 (France), BMBF and DFG (Germany), DAE and DST (India), SFI (Ireland), INFN (Italy), MEXT (Japan), the Korean World Class University Program and NRF (Korea), CONACyT (Mexico), FOM (Netherlands), MON, NRC KI and RFBR (Russia), the Slovak R&D Agency, the Ministerio de Ciencia e Innovación, and Programa Consolider-Ingenio 2010 (Spain), The Swedish Research Council (Sweden), SNSF (Switzerland), STFC and the Royal Society (United Kingdom), and the A.P Sloan Foundation (USA).

APPENDIX: EVALUATION OF SYSTEMATIC UNCERTAINTIES

Systematic uncertainties arise from inadequate modeling of signal and backgrounds and from the inability to reproduce the detector response with simulated events. Systematic uncertainties also arise from ambiguities in reconstructing the top quarks from their jet and lepton remnants. We minimize such uncertainties by using independent data to calibrate the absolute response of the detector, and we use state-of-the-art input from theory for modeling the signal and backgrounds. We use alternative models for signal and different parameters for modeling backgrounds to check our assumptions.

Table VIII lists the uncertainties from the Run II lepton+jets measurements for CDF and D0 that are based on the matrix-element technique [26, 27]. These two measurements provide most of the sensitivity to the combined m_t result and are discussed below. Before explaining how each individual systematic uncertainty is estimated, we will first discuss how the uncertainties from different sources are propagated to m_t and how they are calculated using ensembles of pseudoexperiments.

Uncertainties related to the performance of the detector and calibration of the reconstructed objects, such as JES, the modeling of jets, leptons, and triggers, and calibration of the b-tagging algorithms, are evaluated by shifting the central values of their respective parameters by ±1 standard deviations (σ) that correspond to the uncertainties on each value. This is done using MC $t\bar{t}$ events for $m_t = 172.5$ GeV. The integrations over the matrix element are performed again for each shifted sample and define shifts in m_t that correspond to each independent source of systematic uncertainty. These uncertainties are not determined at other m_t values, and it is assumed that their dependence on m_t is minimal.

For uncertainties that arise from ambiguities in the modeling of the $t\bar{t}$ signal, which include the uncertainties from initial- and final-state radiation, higher-order QCD corrections, b-jet hadronization, light-jet hadronization, the underlying-event model, and color reconnection, we generate simulated $t\bar{t}$ events using alternative models also at $m_t = 172.5$ GeV. These events are processed through detector simulation and are reconstructed, and the probability density is calculated by integration over the matrix elements.

For the uncertainties from the choice of parton distribution functions, the ratio of contribution from quark annihilation and gluon fusion, and models for overlapping interactions, we reweight the fully reconstructed simulated $t\bar{t}$ MC events at $m_t = 165, 170, 172.5, 175$, and 180 GeV to reflect the uncertainty on the ±1σ range on each parameter and extract its impact on m_t.

Each method used to measure m_t is calibrated using $t\bar{t}$ MC events generated at $m_t = 165, 170, 172.5, 175, 180$ GeV, which provide the relationship between input and "measured" masses. A straight line is fitted to these values, representing a response function that is used to correct the m_t measurement in data.

Systematic uncertainties are evaluated using studies of ensembles of pseudoexperiments. For each of the shifted or reweighted sets of events, and those based on alternative models or different generated m_t, we create an ensemble of at least 1000 pseudoexperiments, by means of binomially smeared signal and background fractions that match the expectation in the data sample and with the total number of events in each pseudoexperiment equal to the number of events observed in data. We use the ensembles of such pseudoexperiments to assess the difference between generated and measured mass and to calibrate the method of mass extraction.

For the uncertainty on background, we change the fraction of background events in the pseudoexperiments within their uncertainties and remeasure the top-quark mass.

For the BLUE combination method, the uncertainties must be defined symmetrically around the central mass value, and this requirement determines part of the following definitions of uncertainty.

TABLE VIII: Individual components of uncertainty on CDF and D0 m_t measurements in the lepton+jets channel for Run II data [26, 27].

Systematic Source	Uncertainty [GeV]	
	CDF (5.6 fb^{-1}) $m_t = 173.00$ GeV	D0 (3.6 fb^{-1}) $m_t = 174.94$ GeV
DETECTOR RESPONSE		
Jet energy scale		
Light-jet response (1)	0.41	n/a
Light-jet response (2)	0.01	0.63
Out-of-cone correction	0.27	n/a
Model for b jets	0.23	0.07
Semileptonic b decay	0.16	0.04
b-jet hadronization	0.16	0.06
Response to $b/q/g$ jets	0.13	0.26
In situ light-jet calibration	0.58	0.46
Jet modeling	0.00	0.36
Jet energy resolution	0.00	0.24
Jet identification	0.00	0.26
Lepton modeling	0.14	0.18
MODELING SIGNAL		
Signal modeling	0.56	0.77
Parton distribution functions	0.14	0.24
Quark annihilation fraction	0.03	n/a
Initial and final-state radiation	0.15	0.26
Higher-order QCD corrections	n/a	0.25
Jet hadronization and underlying event	0.25	0.58
Color reconnection	0.37	0.28
Multiple interactions model	0.10	0.05
MODELING BACKGROUND		
Background from theory	0.27	0.19
Higher-order correction for heavy flavor	0.03	0.07
Factorization scale for W+jets	0.07	0.16
Normalization to predicted cross sections	0.25	0.07
Distribution for background	0.07	0.03
Background based on data	0.06	0.23
Normalization to data	0.00	0.06
Trigger modeling	0.00	0.06
b-tagging modeling	0.00	0.10
Signal fraction for calibration	n/a	0.10
Impact of multijet background on the calibration	n/a	0.14
METHOD OF MASS EXTRACTION		
Calibration method	0.10	0.16
STATISTICAL UNCERTAINTY	0.65	0.83
UNCERTAINTY ON JET ENERGY SCALE	0.80	0.83
OTHER SYSTEMATIC UNCERTAINTIES	0.67	0.94
TOTAL UNCERTAINTY	1.23	1.50

For the uncertainties obtained in ensemble studies with shifted or reweighted parameters, m_t^+ corresponds to the $+1\sigma$ shift in the input parameter and m_t^- corresponds to the -1σ shift. The systematic uncertainty on the value of m_t from these parameters is defined as $\pm |m_t^+ - m_t^-|/2$, unless both shifts are in the same direction relative to the nominal value, in which case the systematic uncertainty is defined as the larger of $|m_t^+ - m_t|$ or $|m_t^- - m_t|$.

For the values obtained from a comparison between two or more models, the systematic uncertainty is taken as $\pm$ of the largest difference among the resulting masses (without dividing by two).

1. Jet energy scale

The following seven terms (1.1 - 1.7) refer to the jet energy scale

1.1 Light-jet response (1)

This uncertainty includes the absolute calibration of the CDF JES for Run I and Run II and the smaller effects on JES from overlapping interactions and the model for the underlying event.

CDF's calibration of the absolute jet energy scale uses the single-pion response to calibrate jets in data and to tune the model of the calorimeter in the simulation. Uncertainties of these processes form the greatest part of the JES uncertainty. Small constant terms are added to account for the model of jet fragmentation and for calorimeter simulation of electromagnetically decaying particles, and to take into account small variations of the absolute calorimeter response over time. The total resulting uncertainty on the absolute JES is 1.8% for 20 GeV jets rising to 2.5% for 150 GeV jets.

At high Tevatron instantaneous luminosities, more than one $p\bar{p}$ interaction occurs during the same bunch crossing, and the average number of interactions depends linearly on instantaneous luminosity and is changed from ≈ 1 to 8 between the start and the end of Run II. If the final-state particles from these extra $p\bar{p}$ interactions overlap with the jets from a $t\bar{t}$ event, the energy of these jets is increased, thereby requiring the correction. The uncertainty on this correction depends on vertex-reconstruction efficiency and the rate for misidentifying vertices. The impact of these effects is checked on data samples, including $W \rightarrow e\nu$, minimum bias, and multijet events with a trigger threshold of 100 GeV. CDF finds an uncertainty of 0.05 GeV per jet. This uncertainty was estimated early in Run II. With increasing instantaneous luminosity, this correction was insufficient, and another systematic uncertainty term was introduced through the "multiple-interactions-model" term, which is described later.

CDF includes the impact of the underlying event on JES in this component of uncertainty. The proton and antiproton remnants of the collision deposit energy in the calorimeter, and these can contribute to the energy of the jets from $t\bar{t}$ decay, which must be subtracted before m_t can be measured accurately. CDF compares the "Tune A" underlying-event model [73] in PYTHIA [69] with the JIMMY model [85, 86] in HERWIG [87] using isolated tracks with $p_T > 0.5$ GeV. The data agree well with Tune A, which is expected since it was tuned to CDF data, but differ from JIMMY by about 30%. This difference is propagated to the absolute calibration of JES and yields a 2% uncertainty for low-p_T jets and less than 0.5% for 35 GeV jets.

MC $t\bar{t}$ events are generated by CDF with jet energies shifted by the above three uncertainties, and the resulting shifts in m_t are used to estimate the uncertainty. The overall uncertainty on m_t from these combined sources is 0.24% for lepton+jets, 0.22% for alljets, 1.18% for CDF Run II dilepton data, and 0.26% for $\not{E}_T$+jets for Run II data of CDF.

1.2 Light-jet response (2)

This uncertainty term represents almost all parts of D0 Run I and Run II calibrations of JES. The absolute energy scale for jets in data is calibrated using γ+jet data with photon $p_T > 7$ GeV and $|\eta_\gamma| < 1.0$, and jet $p_T > 15$ GeV and $|\eta_{jet}| < 0.4$, using the "$\not{E}_T$ projection fraction" method [84]. Simulated samples of γ+jets and Z+jets events are compared to data and used to correct the energy scale for jets in MC events. The JES is also corrected as a function of η for forward jets relative to the central jets using γ+jets and dijets data. Out-of-cone particle scattering corrections are determined with γ+jets data and simulated events, without using overlays of underlying events, to avoid double counting of this effect. Templates of deposited energy are formed for particles belonging to and not belonging to a jet using 23 annular rings around the jet axis for $\mathcal{R}(y, \phi) =$

$\sqrt{(\Delta y)^2 + (\Delta \phi)^2} \leq 3.5$. All of these calibration steps are combined, and the total uncertainty on JES is calculated for light jets and heavy-flavor jets (independent of the type of jet). The resulting D0 uncertainty on m_t for Run II lepton+jets events is 0.36% and 0.86% for dilepton data.

This uncertainty term also includes the relative jet energy correction as a function of jet η for CDF. This is measured using dijet data, along with PYTHIA and HERWIG simulations of $t\bar{t}$ events generated with shifted jet energies, and lead to the following uncertainties on Run II measurements of m_t: 0.01% for lepton+jets, 0.02% for alljets, 0.34% for dileptons, and 0.03% for $\not{E}_T$+jets.

1.3 Out-of-cone corrections

For all CDF measurements and for D0 Run I, this uncertainty component accounts for energy lost outside the jet reconstruction cone and uses the difference between two models of light-quark and gluon fragmentation and simulation of the underlying event. D0 changed the way it measures the out-of-cone uncertainty between Run I and Run II, and this uncertainty for D0 Run II measurements is therefore included in the light-jet response (2) term, described previously.

Energy is lost from the cone of jet reconstruction when a quark or gluon is radiated at a large angle relative to the original parton direction, or when the fragmentation shower is wider than the cone, or when low momentum particles are bent out of the cone by the axial magnetic field of the detector. Energy is gained in the cone from initial-state radiation and from remnants of spectator partons, called collectively at CDF the underlying event. The two models compared by CDF in Run II are PYTHIA with Tune A for the underlying event and HERWIG with the JIMMY modeling of the underlying event. For the narrow cone size of $\mathcal{R} = 0.4$ used in measurements of m_t, more energy is lost from the cone than gained. The correction is measured using PYTHIA dijet events and data in the region $0.4 < \mathcal{R} \leq 1.3$. A small constant is added to compensate for energy outside the $\mathcal{R} > 1.3$ region ("splash out"). The correction is largest for jets at low transverse momentum: +18% for $p_T = 20$ GeV jets and < 4% for jets with $p_T > 70$ GeV. A detailed description of the method can be found in Ref. [83].

The uncertainty on these corrections is measured by comparing γ + jets data to the two simulations. The largest difference between either of the models and data is taken as the uncertainty (the difference between the two models is very small). For jets with $p_T = 20$ GeV, the uncertainty on the jet energy scale is 6%, and for jets above 70 GeV, it is 1.5%. These translate into uncertainties on CDF Run II m_t measurements of 0.16% for the lepton+jets measurement, 0.14% for alljets, 1.25% for dileptons, and 0.12% for $\not{E}_T$+jets.

1.4 Energy offset

This uncertainty term is specific to D0 Run I

measurements. It includes the uncertainty arising from uranium decays noise in the calorimeter and from the correction for multiple interaction to JES. These lead to uncertainties in m_t of 0.72% for lepton+jets and 0.77% for dilepton events. In Run II, the integration time for the calorimeter electronics is short, after the upgrade to shorter bunch-crossing time (3.5 μs to 396 ns). This effect results in a negligible uncertainty on the offset for D0 Run II measurements of m_t.

1.5 Model for b jets

(i) *Semileptonic b decay*

The uncertainty on the semileptonic branching fraction $(10.69 \pm 0.22) \times 10^{-2}$ (PDG 2007 values) of B hadrons affects the value of m_t. Both collaborations reweight $t\bar{t}$ events by $\pm$ the uncertainty on the central value ($\pm$2.1%), and take half the resulting mass difference as the uncertainty on m_t: 0.09% for CDF and 0.03% for D0.

(ii) *b-jet hadronization*

For its nominal m_t measurements, CDF uses the default PYTHIA model of b-jet fragmentation based on the Bowler model [88] ($r_q = 1.0$, $a = 0.3$, $b = 0.58$), where r_q is the Bowler fragmentation-function parameter and a and b are Lund fragmentation-function parameters. D0 uses a model with these parameters tuned to data from ALEPH, DELPHI, and OPAL [89] ($r_q = 0.897 \pm 0.013$, $a = 1.03 \pm 0.08$, $b = 1.31 \pm 0.08$). To measure the uncertainty on these models, CDF compares its m_t values to those measured with the LEP parameters used by D0, and to those from the SLD experiment at SLC [89] ($r_q = 0.980 \pm 0.010$, $a = 1.30 \pm 0.09$, $b = 1.58 \pm 0.09$). D0 compares the measured m_t with the LEP parameters to the one from SLC. The resulting uncertainties on the m_t extracted from the lepton+jets channel are 0.09% for CDF and 0.03% for D0.

For some analyses, the determination of the uncertainties in (i) and (ii) may be affected by statistical fluctuations of the MC samples.

1.6 Response to $b/q/g$ jets

The calibrations of JES described in the first two paragraphs of the Appendix are derived on samples dominated by "light-quark" and gluon jets and applied to all jets. However, the calorimeter response to heavy-flavor jets differs in that these particles often decay semileptonically, and the b jet will have some energy lost through the escaping neutrino. Bottom quark jets can also contain an electron that showers in a pattern different than for hadronic particles, or the jet may contain a muon that neither produces a shower nor gets absorbed in the calorimeter. Bottom jets also differ from light jets in the distribution of their shower and particle content. Since every $t\bar{t}$ event contains two b jets, it is important to understand their energy calibration after the application of the previous overall corrections.

CDF measures an uncertainty from the difference between the b-jets response and light-flavor jets response in Run II. CDF takes sets of MC $t\bar{t}$ events and cluster particles into jets classifying each such particle jet as a b jet or a light jet [81]. Single-particle response for data and for MC events are applied to the formed particle jets to predict the energy measured in the calorimeter. A double ratio is calculated: $(p_T^{\text{data}}/p_T^{\text{MC}})_{b \text{ jets}}/(p_T^{\text{data}}/p_T^{\text{MC}})_{\text{light jets}}$, which is found to be 1.010. The uncertainty on m_t is measured by generating new $t\bar{t}$ samples with the b-jet scale shifted by this 1% difference, which results in 0.1% uncertainty in m_t for the lepton+jets measurement.

For Run II measurements, D0 corrects the transverse-momentum distributions of jets differently in four regions of detector pseudorapidity to make the MC response match that in data (after the main JES calibration) as a function of jet flavor: b jets, light-quark jets (u, d, s, c), and gluon jets [27]. The correction functions are shifted up and down by their uncertainties, and the extracted shifts in m_t are used to define the resulting uncertainty on m_t of 0.15% for the lepton+jets measurement and 0.23% for the dilepton measurement.

1.7 *In situ* light-jet calibration

In $t\bar{t}$ events where one or both W bosons decay to $q\bar{q}'$, the world average value of M_W [7] is used to constrain the jet energy scale for light-quark jets *in situ* [90, 91]. CDF and D0 perform simultaneous measurements of m_t and M_W, and fit a linear function to the JES for light-quark jets that is applied to all the jets to improve precision of m_t.

CDF measures the *in situ* rescaling factor independently in their lepton+jets, alljets, and $\slashed{E}_T$+jets analyses, and so these terms are uncorrelated. D0 applies the rescaling derived from their lepton+jets measurement to dilepton events, and these uncertainties are therefore correlated.

The uncertainty from the *in situ* calibration is determined through a two-dimensional minimization of a likelihood that is a function of top-quark mass and JES. The extracted JES is then shifted relatively to its measured central value, and a one-dimensional fit is performed to the top-quark mass. The difference in quadrature between the uncertainty on m_t from the first and second fits is taken as the uncertainty on m_t from the *in situ* calibration, giving 0.34% for CDF's lepton+jets measurement, 0.27% for D0's lepton+jets result, 0.55% for CDF's alljets, 0.89% for their $\slashed{E}_T$+jets measurement, and 0.32% for D0's dilepton measurement.

2. Jet modeling

Applying jet algorithms to MC events, CDF finds that the resulting efficiencies and resolutions closely match those in data. The small differences propagated to m_t lead to a negligible uncertainty of 0.005 GeV, which is then ignored. D0 proceeds as follows.

(i) *Jet energy resolution*

The modeling of the jet energy resolution is corrected in D0 to match that in data. The value of m_t is then remeasured using MC samples with jet energy resolution corrections shifted up and down by their uncertainties, resulting in an uncertainty on m_t of 0.18%.

(ii) *Jet identification*

D0 applies correction functions to MC events to match the jet identification efficiency in data. The uncertainty on m_t is estimated by reducing the corrections by 1σ and remeasuring the mass in the adjusted MC samples. The efficiency can only be shifted down and not up because jets can be removed from the simulated events but not added. The uncertainty on m_t is therefore set to $\pm$ the single-sided shift and is 0.15%.

3. Lepton modeling

(i) *Momentum scale for leptons*

In Run II, the electron and muon channels for CDF and the muon channels for D0 are used to calibrate the lepton momentum scales by comparing the invariant dilepton mass $m_{\ell 1 \ell 2} = \sqrt{(E_{\ell 1} + E_{\ell 2})^2 - (p_{\ell 1} + p_{\ell 2})^2}$ for $J/\psi \to \ell\ell$ and $Z \to \ell\ell$ decays in MC events with data. The positions of the resonances observed in the $m_{\ell\ell}$ distributions reflect the absolute momentum scales for the leptons. CDF and D0 perform a linear fit as a function of the mean value of transverse momentum to the two mass points (3.0969 GeV and 91.1876 GeV [7]), assuming that any mismatch is attributable to an uncertainty in the calibration of the magnetic field. D0 also fits a quadratic relation, assuming that the difference in scale arises from misalignment of the detector. The value of m_t is measured using MC $t\bar{t}$ ensembles without rescaling lepton p_T and with lepton p_T values rescaled using these fitted relations. Half of the largest difference in extracting m_t is taken as its systematic uncertainty resulting from the lepton p_T scale. For muon measurements from D0, the largest shift is observed for the linear parametrization. In Run I, this source of uncertainty was neglected as it was negligible relative to other sources of uncertainty.

In D0 Run II measurement of the W-boson mass in the electron decay channel, it was found that 0.26 radiation length of material was left out in the GEANT modeling of the solenoid [92]. The Z-boson mass peak was used to calculate a quadratic correction to the electron energy by comparing MC events generated with additional solenoid material to data. This correction was then propagated to the m_t measurement.

The uncertainties on the m_t measurements from the lepton momentum scale are 0.08% for CDF lepton+jets measurements and 0.10% for D0, and 0.16% for CDF dilepton measurements and 0.28% for D0 dilepton results.

(ii) *Lepton momentum resolution*

The muon momenta in simulated events at D0 are smeared to match the resolution in data. The uncertainty on this correction corresponds to an uncertainty on m_t of 0.17%.

4. Signal modeling

(i) *Parton distribution functions*

In Run I, the uncertainties from choice of PDF are determined by measuring the change in m_t using the MRSA$'$ set [93] instead of MRSD$'_0$ [65] or CTEQ4M [66], and are found to be negligible.

In Run II, the uncertainty is measured by CDF by comparing CTEQ5L results with MRST98L [94], by changing the value of α_s in the MRST98L model, and by varying the 20 eigenvectors in CTEQ6M [9]. The total uncertainty is obtained by combining these sources in quadrature. D0 measures this uncertainty by reweighting the PYTHIA model to match possible excursions in the parameters represented by the 20 CTEQ6M uncertainties and taking the quadratic sum of the differences. The resulting uncertainty on m_t is 0.08% for CDF and 0.14% for D0.

(ii) *Fractional contributions from quark annihilation and gluon fusion*

In Run I, this source of uncertainty in $t\bar{t}$ production is not considered. In Run II, CDF estimates the effect on m_t by reweighting the gluon fusion fraction in the PYTHIA model from 5% to 20% [95]. The uncertainty on m_t is found to be 0.02%. This uncertainty is included by D0 in the systematic component (iv) below, where the effects of higher-order QCD corrections are discussed.

(iii) *Initial- and final-state radiation*

Initial- and final-state radiation refers to additional gluons radiated from the incoming or outgoing partons or from the top quarks. Jets initiated by these gluons affect the measured value of m_t because they can be misidentified as jets from the final-state partons in top-quark decay. Extensive checks were performed in Run I measurements to assess the effects of initial- and final-state radiation by varying parameters in HERWIG.

In Run II, uncertainties from initial- and final-state radiation are assessed by both collaborations using a CDF measurement [96] in Drell-Yan dilepton events that have the same $q\bar{q}$ initial state as most $t\bar{t}$ events, but no final-state radiation. The mean p_T of the produced dilepton pairs is measured as a function of the dilepton invariant mass, and the values of Λ_{QCD} and the Q^2 scale in the MC that matches best the data when extrapolated to the $t\bar{t}$ mass region are found. CDF's best-fit values are Λ_{QCD} (5 flavors) = 292 MeV with $0.5 \times Q^2$ and Λ_{QCD} (5 flavors) = 73 MeV with $2.0 \times Q^2$ for $\pm\sigma$ excursions around the mean dilepton p_T values. Since the initial and final-state shower algorithms are controlled by the same QCD evolution equation [67], the same variations of Λ_{QCD} and Q^2 scale are used to estimate the effect of final-state radiation. The resulting uncertainty for

modeling of the initial- and final-state radiation is 0.09% for CDF and 0.15% for D0. The correction algorithm does not distinguish between "soft" (out-of-cone) and "hard" (separate jet) radiation, and there is therefore some overlap between the uncertainty on m_t for the out-of-cone jet energy correction and for gluon radiation. There is also some overlap between the uncertainty for initial- and final-state radiation and the uncertainty on higher-order QCD corrections for high-p_T radiation.

(iv) *Higher-order QCD corrections*

Higher-order QCD corrections to $t\bar{t}$ production are not used for Run I measurements, as only LO generators were available at that time. D0 measures higher-order jet-modeling uncertainties in Run II by comparing m_t extracted with ALPGEN and HERWIG for evolution and fragmentation to the value obtained from events generated with MC@NLO [8], which uses HERWIG parton showering with a NLO model for the hard-scattering process. This component of uncertainty also includes (for D0) the uncertainty from the fraction of quark-antiquark to gluon-gluon contributions to the initial state. CDF also studies differences in m_t using MC@NLO and finds that the uncertainties in distributions in the number of jets and the transverse momentum of the $t\bar{t}$ system overlap with the uncertainty from initial- and final-state radiation. Future measurements of m_t are expected to treat these uncertainties separately. The uncertainty on m_t from higher-order contributions and initial-state $q\bar{q}/gg$ ratio is 0.14% for D0.

(v) *Jet hadronization and underlying event*

In Run I, CDF measured the uncertainty in the model for parton showering and hadronization and the underlying-event by comparing the value of m_t based on HERWIG to that on PYTHIA [97], and D0 compared HERWIG results to those from ISAJET [98].

In Run II, CDF estimates these uncertainties by comparing m_t obtained using PYTHIA with Tune A of the underlying-event model to results from HERWIG with a tuned implementation of the underlying-event generator JIMMY. D0 estimates these uncertainties by comparing identical sets of hard-scatter events from ALPGEN coupled to HERWIG instead of to PYTHIA. For the uncertainty on m_t, this corresponds to 0.40% for CDF and 0.33% for D0.

(vi) *Color reconnection*

There are up to six final-state quarks in $t\bar{t}$ events, in addition to initial and final-state radiation. When hadronization and fragmentation occur, there are color interactions among these partons and the color-remnants of the proton and antiproton. This process is referred to as "color reconnection". It changes the directions and distributions of final-state jets [99, 100], which affects the reconstructed value of m_t [74].

The uncertainty on color reconnection was not evaluated for Run I because appropriate MC tools were not available at that time. Both collaborations estimate this effect in Run II by comparing the value of m_t extracted from ensembles of $t\bar{t}$ events generated by PYTHIA using the difference between two parton shower simulations: (i) angular ordering for jet showers (same as used in the nominal m_t measurements) using the A-PRO underlying-event model (Tune A but updated using the "Professor" tuning tool [101]), and (ii) ACR-PRO. ACR-PRO is identical to A-PRO except that it includes color reconnection in the model. The resulting uncertainties on m_t are 0.32% for CDF and 0.16% for D0.

5. Multiple interactions model

Monte Carlo simulated events are overlaid with Poisson-distributed low-p_T events (PYTHIA MC events for CDF, "zero-bias" data for D0) to simulate the presence of simultaneous additional $p\bar{p}$ interactions. The mean number of overlaid events is chosen at the time of event generation, but in data, the number of such interactions changes with instantaneous luminosity of the Tevatron.

CDF measures m_t as a function of the number of multiple interactions, finding a change of 0.07 ± 0.10 GeV per primary vertex. For CDF's measurements, the average number of primary vertices in data is 2.20 and for simulated events it is 1.85, leading to an uncertainty on m_t of 0.02%. CDF adds to this in quadrature a term to cover the difference in jet energy response as a function of the number of multiple interactions of 0.06%, giving a total uncertainty of 0.06%.

D0 reweights the simulated events to make the instantaneous luminosity distribution match that in data. The resulting uncertainty on m_t is 0.03%.

6. Background from theory

(i) *Higher-order correction for heavy flavor*

D0 corrects the leading-log W+jets cross section from ALPGEN to NLO precision before normalizing this background to data. This increases the fraction of $Wb\bar{b}$ and $Wc\bar{c}$ events in W+jets by a factor of 1.47 ± 0.50. CDF normalizes the W+heavy-flavor jets background to data independent of the other components in W+jets, which has a similar effect. The resulting uncertainties on m_t are 0.11% for CDF and 0.04% for D0.

(ii) *Factorization scale for W+jets*

The transverse momenta of the jets in W+jets events are sensitive to the factorization and renormalization scales chosen for the calculations. These two scales are set equal to each other, with $Q^2 = M_W^2 + \sum p_T^2$. To determine the uncertainty on m_t, the scale is changed from $(Q/2)^2$ to $(2 \times Q)^2$, the MC events regenerated, and the mass remeasured. Changing the scale does not affect the fraction of W+jets in the model but does affect the transverse-momentum distributions of the jets. The uncertainties on m_t are 0.02% for CDF and 0.09% for D0.

(iii) *Normalization to predicted cross sections*

CDF divides the background into seven independent parts: W+heavy-flavor jets, W + light-flavor jets, single-top tqb and tb, Z+jets, dibosons (WW, WZ, and ZZ), and multijet contributions. This uncertainty term covers the normalization of the components modeled with MC simulated events (not multijets). The small backgrounds from single-top, Z+jets, and diboson production are normalized to NLO calculations. The uncertainties on the cross sections are 10% for tqb, 12% for tb, 14% for Z+jets, and 10% for dibosons. The W+jets background is normalized to data before implementation of b tagging, using a fit to the distribution for $\not{E}_T$ in the event. The uncertainty on this normalization cannot easily be disentangled from the other sources, and so it is kept in this category. The combined uncertainty on m_t from these normalizations is 0.09%.

D0 also normalizes single-top, Z+jets, and diboson contributions, in all analysis channels, and Drell-Yan in the dilepton channel, to next-to-leading-order cross sections, using values from the MCFM event generator [102]. The uncertainties on the cross sections take into account the uncertainty on the PDF and on the choice of factorization and renormalization scales, which together propagate through to m_t an uncertainty of 0.04%.

(iv) *Background differential distributions*

For CDF, different methods were used to estimate the uncertainty attributable to the overall background shape. In the recent lepton+jets analysis, this uncertainty was assessed by dividing randomly the background events into subsets, building the background likelihood from one of the subsets, and reconstructing the m_t from the second subset. In the next step, the difference in m_t obtained from the second subset and the nominal m_t value is evaluated. This contributes an uncertainty of 0.03%. CDF also estimates an uncertainty from the limited MC statistics used to measure the background. This yields an additional 0.03% uncertainty on m_t.

For D0, the p_T and η distributions of jets in W+jets events do not fully reproduce those in data. An uncertainty to cover these deviations is based on the difference between the model for background and data in the η distribution of the third jet in three-jet events. The resultant uncertainty on m_t is 0.09%.

7. Background based on data

(i) *Normalization to data*

In the lepton+jets, alljets, $\not{E}_T$+jets, and decay-length channels, backgrounds from multijet events are normalized to data. In the lepton+jets analyses at D0, the W+jets background model is combined with the contribution from multijet events, and both are normalized simultaneously to data, so that their uncertainties in normalization are anticorrelated. In dilepton analyses at CDF, the Drell-Yan background is normalized to data. For the lepton+jets analyses, CDF uncertainty on m_t from the normalization of the multijet backgrounds to data is 0.03%, and D0's uncertainty for the normalization of W+jets and multijets to data is 0.13%.

(ii) *Trigger modeling*

CDF expects a negligible uncertainty on m_t from the modeling of the trigger. D0 simulates the trigger turn-on efficiencies for MC events by applying weights as a function of the transverse momentum of each object in the trigger. The uncertainty is measured by setting all the trigger efficiencies to unity and recalculating the value of m_t, which shifts m_t by 0.03%.

(iii) *b-tagging modeling*

CDF applies the b-tagging algorithm directly to MC events and finds that any difference between the b-tagging behavior in MC and data has a negligible impact on the measurement of m_t. D0 applies the b-tagging algorithm directly to MC events for recent Run II measurements. Previously b-tagging was simulated with tag probability, and in Run I, as D0 did not have a silicon tracker, nonisolated muons were used to identify b jets. The tagging efficiency for simulated events is made to match that in data by randomly dropping b tags for b and c jets, while assigning a per jet weight for tagging light-flavor jets as b jets. The uncertainties for these corrections are determined by shifting the efficiencies for tagging b and c jets by 5% and by 20% for light jets, which introduces an uncertainty on m_t of 0.06%.

(iv) *Signal fraction for calibration*

D0 measures the impact of the uncertainty in the ratio of signal to background events, which affects the calibration of m_t. Changing the signal fraction within uncertainty results in an uncertainty on m_t of 0.06%.

(v) *Impact of multijet background on the calibration*

Multijet background events are not used in D0 samples that determine the calibration of m_t for the lepton+jets measurement since the background probability for such events is much larger than the signal probability. The assumption that this has a small effect on m_t is tested by selecting a multijet-enriched sample of events from data (by inverting the lepton isolation criteria) and adding these events when deriving the calibration. Applying this alternative calibration to data indicates that m_t can shift by an uncertainty of 0.08%.

8. Calibration method

Monte Carlo $t\bar{t}$ ensembles are generated at different values of input m_t ($m_t = 165, 170, 172.5, 175, 180$ GeV), and calibrations relate the input masses for $t\bar{t}$ events to the extracted masses using a straight line. For some of the m_t measurements, there is an additional *in situ* calibration of the JES to the light quarks in W-boson decay, which is then applied to all jets. The uncertainties

from both calibrations are propagated to the uncertainty on m_t, which for CDF are 0.04% and 0.05%, respectively, giving a total of 0.06%. For D0, the uncertainty on m_t is 0.13%.

[1] M. Kobayashi and T. Maskawa, Prog. Theor. Phys. **49**, 652 (1973).

[2] J.H. Christenson, J.W. Cronin, V.L. Fitch, and R. Turlay, Phys. Rev. Lett. **13**, 138 (1964).

[3] F. Abe *et al.* (CDF Collaboration), Phys. Rev. D **50**, 2966 (1994); F. Abe *et al.* (CDF Collaboration), Phys. Rev. Lett. **73**, 225 (1994).

[4] F. Abe *et al.* (CDF Collaboration), Phys. Rev. Lett. **74**, 2626 (1995).

[5] S. Abachi *et al.* (D0 Collaboration), Phys. Rev. Lett. **74**, 2632 (1995).

[6] N. Cabibbo, Phys. Rev. Lett. **10**, 531 (1963).

[7] K. Nakamura *et al.* (Particle Data Group), J. Phys. G **37**, 075021 (2010).

[8] S. Frixione and B.R. Webber, arXiv:0812.0770 [hep-ph].

[9] J. Pumplin, D.R. Stump, J. Huston, H.-L. Lai, P. Nadolsky, and W.-K. Tung, J. High Energy Phys. 07, 012 (2002).

[10] F. Englert and R. Brout, Phys. Rev. Lett. **13**, 321 (1964); P.W. Higgs, Phys. Lett. **12**, 132 (1964); P.W. Higgs, Phys. Rev. Lett. **13**, 508 (1964); G.S. Guralnik, C.R. Hagen, and T.W.B. Kibble, Phys. Rev. Lett. **13**, 585 (1964); P.W. Higgs, Phys. Rev. **145**, 1156 (1965).

[11] U. Langenfeld, S. Moch, and P. Uwer, Phys. Rev. D **80**, 054009 (2009).

[12] M.C. Smith and S.S. Willenbrock, Phys. Rev. Lett. **79**, 3825 (1997).

[13] A. Buckley *et al.*. Phys. Rept. **504**, 145 (2011).

[14] V.M. Abazov *et al.* (D0 Collaboration), Phys. Lett. B **703**, 422 (2011).

[15] V.M. Abazov *et al.* (D0 Collaboration), Phys. Rev. Lett. **103**, 132001 (2009); Phys. Rev. D **84**, 052005 (2011).

[16] T. Aaltonen *et al.* (CDF Collaboration), Phys. Rev. Lett. **106**, 152001 (2011).

[17] S. Chatrchyan *et al.* (CMS Collaboration), J. High Energy Phys. 1206, 109 (2012).

[18] The ALEPH, CDF, D0, DELPHI, L3, OPAL, SLD Collaborations, the LEP Electroweak Working Group, the Tevatron Electroweak Working Group, and the SLD Electroweak and Heavy Flavor Groups, arXiv:1012.2367 [hep-ex]. `http://lepewwg.web.cern.ch/LEPEWWG/`

[19] private communication with S. Heinemeyer based on S. Heinemeyer, W. Hollik, and G. Weiglein, Phys. Rept. **425**, 265 (2006). `http://www.ifca.es/users/heinemey/uni/plots/`

[20] M. Baak, M. Goebel, J. Haller, A. Hoeker, D. Ludwig, K. Mönig, M. Schott, and J. Stelzer, Eur. Phys. J. C **72**, 2003 (2012). `http://cern.ch/gfitter/`

[21] C. Quigg, Physics Today **50N5**, 20 (May 1997), arXiv:hep-ph/9704332, and references therein.

[22] The LEP Collaborations ALEPH, DELPHI, L3, OPAL and the LEP Electroweak Working Group. CERN-PPE/94-187 (1994). and references therein.

[23] S. Chatrchyan *et al.* (CMS Collaboration), J. High Energy Phys. 1107, 049 (2011).

[24] G. Aad *et al.* (ATLAS Collaboration), Eur. Phys. J. C **72**, 2046 (2012).

[25] J.C. Estrada Vigil, Ph.D. thesis, University of Rochester, 2001, FERMILAB-THESIS-2001-07.

[26] T. Aaltonen *et al.* (CDF Collaboration), Phys. Rev. Lett. **105**, 252001 (2010).

[27] V.M. Abazov *et al.* (D0 Collaboration), Phys. Rev. D **84**, 032004 (2011).

[28] A.B. Galtieri, F. Margaroli, and I. Volobouev, Rep. Prog. Phys. **75** 056201 (2012); G.V. Velev, J. of Phys. Conf. Ser. **323** 012010 (2011); F. Deliot and D. A. Glenzinski, Rev. Mod. Phys. **84**, 211 (2012); D. Wicke, Eur. Phys. J. C **71**, 1627 (2011).

[29] V.M. Abazov *et al.* (D0 Collaboration), Phys. Rev. D **84**, 012008 (2011); Phys. Lett. B **704**, 403 (2011); Phys. Rev. D **82**, 071102 (2010); T. Aaltonen *et al.* (CDF Collaboration), Phys. Rev. D **83**, 071102 (2011); **84**, 031101 (2011); **82**, 052002 (2010); **81**, 052011 (2010); **84**, 032003 (2011).

[30] P.M. Nadolsky, H.-L. Lai, Q.-H. Cao, J. Huston, J. Pumplin, D. Stump, W.-K. Tung, and C.-P. Yuan, Phys. Rev. D **78**, 013004 (2008); S. Moch and P. Uwer, Phys. Rev. D **78**, 034003 (2008); M. Cacciari, S. Frixione, M.L. Mangano, P. Nason, and G. Ridolfi, J. High Energy Phys. 0809, 127 (2008); N. Kidonakis and R. Vogt, Phys. Rev. D **78**, 074005 (2008); V. Ahrens, A. Ferroglia, M. Neubert, B.D. Pecjak, and L.L. Yang, J. High Energy Phys. 1009, 097 (2010); N. Kidonakis, Phys. Rev. D **82**, 114030 (2010); V. Ahrens, A. Ferroglia, M. Neubert, B.D. Pecjak, and L.L. Yang, Phys. Lett. B **703**, 135 (2011); M. Cacciari, M. Czakon, M. L. Mangano, A. Mitov and P. Nason, Phys. Lett. B **710**, 612 (2012); M. Beneke, P. Falgari, S. Klein and C. Schwinn, Nucl. Phys. B **855**, 695 (2012); M. Beneke, P. Falgari, S. Klein, J. Piclum, C. Schwinn, M. Ubiali and F. Yan, J. High Energy Phys. 1207, 194 (2012); P. Baernreuther, M. Czakon and A. Mitov, arXiv:1204.5201 [hep-ph].

[31] V.M. Abazov *et al.* (D0 Collaboration), Phys. Lett. B **693**, 515 (2010).

[32] T. Aaltonen *et al.* (CDF Collaboration), Phys. Rev. Lett. **102**, 042001 (2009); **105**, 232003 (2010); V.M. Abazov *et al.* (D0 Collaboration), Phys. Rev. Lett. **106**, 022001 (2011); Phys. Rev. D **85**, 091104 (2012).

[33] M. Jeżabek and J.H. Kühn, Phys. Rev. D **48**, 191 (1993).

[34] H. Cramer, *Mathematical Methods of Statistics*, (Princeton University Press, Princeton, 1946), p. 554.

[35] L. Lyons, D. Gibaut, and P. Clifford, Nucl. Instrum. Methods in Phys. Res. Sect. A **270**, 110 (1988).

[36] A. Valassi, Nucl. Instrum. Methods in Phys. Res. Sect. A **500**, 391 (2003).

[37] The Top Averaging Group for the CDF and D0 Collaborations, Fermilab Technical Memo No. 2084 (1999).

[38] The CDF Collaboration, the D0 Collaboration, and the Tevatron Electroweak Working Group, arXiv:hep-ex/040401.

[39] The CDF Collaboration, the D0 Collaboration, and

the Tevatron Electroweak Working Group, Fermilab Technical Memo No. 2323-E (2005), arXiv:hep-ex/0507091.

[40] The Tevatron Electroweak Working Group for the CDF and D0 Collaborations, Fermilab Technical Memo No. 2347-E (2006), arXiv:hep-ex/0603039.

[41] The Tevatron Electroweak Working Group for the CDF and D0 Collaborations, Fermilab Technical Memo No. 2355-E (2006), arXiv:hep-ex/0608032.

[42] The Tevatron Electroweak Working Group for the CDF and D0 Collaborations, Fermilab Technical Memo No. 2380-E (2007), arXiv:hep-ex/0703034.

[43] The Tevatron Electroweak Working Group for the CDF and D0 Collaborations, Fermilab Technical Memo No. 2403-E (2008), arXiv:0803.1683 [hep-ex].

[44] The Tevatron Electroweak Working Group for the CDF and D0 Collaborations, Fermilab Technical Memo No. 2413-E (2008), arXiv:0808.1089 [hep-ex].

[45] The Tevatron Electroweak Working Group for the CDF and D0 Collaborations, Fermilab Technical Memo No. 2427-E (2009), arXiv:0903.2503 [hep-ex].

[46] The Tevatron Electroweak Working Group for the CDF and D0 Collaborations, Fermilab Technical Memo No. 2466-E (2010), arXiv:1007.3178 [hep-ex].

[47] The Tevatron Electroweak Working Group for the CDF and D0 Collaborations, Fermilab Technical Memo No. 2504-E (2011), arXiv:1107.5255 [hep-ex].

[48] T. Affolder *et al.* (CDF Collaboration), Phys. Rev. D **63**, 032003 (2001).

[49] V.M. Abazov *et al.* (D0 Collaboration), Nature **429**, 638 (2004).

[50] T. Aaltonen *et al.* (CDF Collaboration), Phys. Lett. B **714**, 24 (2012).

[51] F. Abe *et al.* (CDF Collaboration), Phys. Rev. Lett. **79**, 1992 (1997); see also Ref. [48] where the systematic uncertainty is reevaluated.

[52] T. Aaltonen *et al.* (CDF Collaboration), Phys. Rev. D **83**, 111101 (2011).

[53] V.M. Abazov *et al.* (D0 Collaboration), submitted to Phys. Rev. D, arXiv:1201.5172 [hep-ex].

[54] F. Abe *et al.* (CDF Collaboration), Phys. Rev. Lett. **82**, 271 (1999); **82**, 2808 (1999) [erratum].

[55] B. Abbott *et al.* (D0 Collaboration), Phys. Rev. Lett. **80**, 2063 (1998); Phys. Rev. D **60**, 052001 (1999).

[56] T. Aaltonen *et al.* (CDF Collaboration), Phys. Rev. Lett. **107**, 232002 (2011).

[57] T. Aaltonen *et al.* (CDF Collaboration), Phys. Rev. D **81**, 032002 (2010).

[58] V.M. Abazov *et al.* (D0 Collaboration), Phys. Lett. B **606**, 25 (2005).

[59] D.E. Acosta *et al.* (CDF Collaboration), Phys. Rev. D **71**, 052003 (2005).

[60] S. Abachi *et al.* (D0 Collaboration), Nucl. Instrum. Methods in Phys. Res. Sect. A **338**, 185 (1994); V.M. Abazov *et al.* (D0 Collaboration), Nucl. Instrum. Methods in Phys. Res. Sect. A **565**, 463 (2006); V.M. Abazov *et al.*, Nucl. Instrum. Methods in Phys. Res. Sect. A **552**, 372 (2005).

[61] S.N. Ahmed *et al.*, Nucl. Instrum. Methods in Phys. Res. Sect. A **634**, 8 (2011); R. Angstadt *et al.*, Nucl. Instrum. Methods in Phys. Res. Sect. A **622**, 298 (2011).

[62] V.M. Abazov *et al.* (D0 Collaboration), Nucl. Instrum. Methods in Phys. Res. Sect. A **620**, 490 (2010).

[63] A. Abulencia *et al.* (CDF Collaboration), Phys. Rev. D **74**, 072006 (2006).

[64] G. Marchesini, B.R. Webber, G. Abbiendi, I.G. Knowles, M.H. Seymour, and L. Stanco, Comput. Phys. Commun. **67**, 465 (1992). In Run I, CDF used version 5.6 and D0 used version 5.7.

[65] A.D. Martin, W.J. Stirling, and R.G. Roberts, Phys. Lett. B **306**, 145 (1993); B **309**, 492 (1993) [erratum].

[66] H.L. Lai, J. Huston, S. Kuhlmann, F. Olness, J. Owens, D. Soper, W.K. Tung, and H. Weerts, Phys. Rev. D **55**, 1280 (1997).

[67] V.N. Gribov and L.N. Lipatov, Sov. J. Nucl. Phys. **15**, 438 (1972); Yu.L. Dokshitzer, Sov. Phys. JETP **46**, 641 (1977); G. Altarelli and G. Parisi, Nucl. Phys. **B126**, 298 (1977).

[68] R. Brun, F. Carminati, and S. Giani, CERN Program Library Long Writeup W5013, 1994 (unpublished).

[69] T. Sjöstrand, S. Mrenna, and P. Skands, J. High Energy Phys. 05, 026 (2006). In Run II, CDF used version 6.216 for top-pairs and diboson generation and version 6.326 for showering, and D0 used version 6.409.

[70] H.-L. Lai, J. Huston, S. Kuhlmann, J. Morfin, F. Olness, J.F. Owens, J. Pumplin, and W.-K. Tung, Eur. Phys. J. C **12**, 375 (2000).

[71] M.L. Mangano, F. Piccinini, A.D. Polosa, M. Moretti, and R. Pittau, J. High Energy Phys. 07, 001 (2003). In Run II, CDF used version 2.10′ and D0 used version 2.11.

[72] S. Höche, F. Krauss, N. Lavesson, L. Lönnblad, M. Mangano, A. Schälicke, and S. Schumann, Proceedings of the Workshop on the Implications of HERA for LHC Physics, edited by A. De Roeck and H. Jung, (DESY, Hamburg, 2005), pp. 288–299, arXiv:hep-ph/0602031.

[73] T. Affolder *et al.* (CDF Collaboration), Phys. Rev. D **65**, 092002 (2002).

[74] P. Skands and D. Wicke, Eur. Phys. J. C **52**, 133 (2007).

[75] F.A. Berends, H. Kuijf, B. Tausk, and W.T. Giele, Nucl. Phys. B **357**, 32 (1991).

[76] F. Maltoni and T. Stelzer, J. High Energy Phys. 02, 027 (2003).

[77] T. Stelzer and W.F. Long, Comput. Phys. Commun. **81**, 357 (1994).

[78] E.E. Boos, V.E. Bunichev, L.V. Dudko, V.I. Savrin, and V.V. Sherstnev, Phys. Atom. Nucl. **69**, 1317 (2006).

[79] E. Boos, V. Bunichev, M. Dubinen, L. Dudko, V. Edneral, V. Ilyin, A. Kryukov, V. Savrin, A. Semenov, and A. Sherstnev, Nucl. Instrum. Methods in Phys. Res. Sect. A **534**, 250 (2004).

[80] The pseudorapidity η is defined as: $\eta = -\ln[\tan(\theta/2)]$, where θ is the polar angle with respect to the proton beamline.

[81] F. Abe *et al.* (CDF Collaboration), Phys. Rev. D **45**, 1448 (1992).

[82] G.C. Blazey *et al.*, Proceedings of the Workshop on QCD and Weak Boson Physics in Run II, edited by U. Baur, R.K. Ellis, and D. Zeppenfeld, pp. 47–77, (Fermilab, Batavia, 2000), FERMILAB-PUB-00-297.

[83] A. Bhatti *et al.*, Nucl. Instrum. Methods in Phys. Res. Sect. A **566**, 375 (2006).

[84] B. Abbott *et al.* (D0 Collaboration), Nucl. Instrum. Methods in Phys. Res. Sect. A **424**, 352 (1999); V. M. Abazov *et al.* (D0 Collaboration), Phys. Rev. D **85**, 052006 (2012).

[85] J.M. Butterworth, J.R. Forshaw, and M.H. Seymour, Z.

Phys. C **72**, 637 (1996).

[86] R. Field and R.C. Group, arXiv:hep-ph/0510198.

[87] G. Corcella, I.G. Knowles, G. Marchesini, S. Moretti, K. Odagiri, P. Richardson, M.H. Seymour, and B.R. Webber, arXiv:hep-ph/0210213. In Run I, CDF and D0 used version 6.5.

[88] M.G. Bowler, Z. Phys. C **11**, 169 (1981).

[89] Y. Peters, K. Hamacher, and D. Wicke, Fermilab Technical Memo No. 2425-E (2006).

[90] A. Abulencia *et al.* (CDF Collaboration), Phys. Rev. D **73**, 032003 (2006).

[91] V.M. Abazov *et al.* (D0 Collaboration), Phys. Rev. D **74**, 092005 (2006).

[92] V.M. Abazov (D0 Collaboration), Phys. Rev. Lett. **108**, 151804 (2012).

[93] A.D. Martin, W.J. Stirling, and R.G. Roberts, Phys. Lett. B **356**, 89 (1995).

[94] A.D. Martin, R.G. Roberts, W.J. Stirling, and R.S. Thorne, Eur. Phys. J C **4**, 463 (1998).

[95] T. Aaltonen *et al.* (CDF Collaboration), Phys. Rev. D **79**, 031101 (2009).

[96] A. Abulencia *et al.* (CDF Collaboration), Phys. Rev. D **73**, 032003 (2006).

[97] T. Sjöstrand, Comput. Phys. Commun. **82**, 74 (1994). In Run I, CDF used version 5.7.

[98] F.E. Paige, S.D. Protopopescu, H. Baer, and X. Tata, BNL-HET-98-18, Brookhaven, 1998 (unpublished). In Run I, CDF used version 6.36 and D0 used version 7.21.

[99] V.M. Abazov *et al.* (D0 Collaboration), Phys. Rev. D **83**, 092002 (2011).

[100] B.R. Webber, J. Phys. G: Nucl. Part. Phys. **24**, 287 (1998).

[101] P. Abreu *et al.* (DELPHI Collaboration), Z. Phys. C **73**, 11 (1996), http://professor.hepforge.org.

[102] J. Campbell, K. Ellis, and C. Williams, Phys. Rev. D **65**, 113007 (2002).